

SAND78-1177
Unlimited Release

The Solar Thermal Test Facility Heliostat Development

D. E. Arvizu

Prepared by Sandia Laboratories, Albuquerque, New Mexico 87185
and Livermore, California 94550 for the United States Department
of Energy under Contract DE-AC04-76DP00789

Printed June 1979



Sandia Laboratories

00 Q(7-73)

***When printing a copy of any digitized SAND
Report, you are required to update the
markings to current standards.***

Issued by Sandia Laboratories, operated for the United States
Department of Energy by Sandia Corporation.

NOTICE

This report was prepared as an account of work sponsored by the United States Government. Neither the United States nor the Department of Energy, nor any of their employees, nor any of their contractors, subcontractors, or their employees, makes any warranty, express or implied, or assumes any legal liability or responsibility for the accuracy, completeness or usefulness of any information, apparatus, product or process disclosed, or represents that its use would not infringe privately owned rights.

Printed in the United States of America

Available from
National Technical Information Service
U. S. Department of Commerce
5285 Port Royal Road
Springfield, VA 22161

Price: Printed Copy \$5.25 ; Microfiche \$3.00

Acknowledgments

Contributions by many people have made this report possible. The author would like to gratefully acknowledge the following:

Heliostat Work

Dean Kuehl
Dave King
Clay Mavis
Harv Shultz
Frank Biggs

Reflectivity

Dick Pettit
Jim Freese
Jerry Myers

Cal-Bar/Computer Support

Dave Davis
Larry Seamons
Roger Aden

Cal-Bar Tests

Roger Aden
Milt Stomp
Tim George
Jim Clark

BCS

Dave King

Reliability/Maintenance/ Focus and Alignment

Bob Edgar
John Holmes

Drafting

Bill Zagar

Helios/Curve Matching

Frank Biggs
Charlie Vittitoe

INTRODUCTION

The heliostat, or solar concentrator, subsystem largely determines the economic and technical effectiveness of a central receiver power plant. Since the cost of the heliostat field accounts for about one-third of the cost of the total power-plant, heliostat design must be economic for this technology to be competitive. One measure of cost-effectiveness is the cost of total annual collected energy.

Because heliostat engineering is relatively new, satisfactory standards for defining specifications are not yet available. In addition, no long-term operational data are available to assess performance. Ideal specifications must include a statement of intended heliostat use and minimal requirements to satisfy those uses. Work is currently under way to establish criteria to define the quality of heliostat performance. The influence on quality of diverse factors such as time of day/year, field location, material type, system construction, and environmental effects shows how difficult such a task is.

This report presents an overview of work funded by the U. S. Department of Energy through Sandia Laboratories for the Solar Thermal Test Facility in Albuquerque, New Mexico, and through the Technical Coordination Office for the Central Power Systems Program in Livermore, California.

Background

In December 1975 four potential suppliers responded to a request for quote (RFQ) to provide the STTF with a heliostat array and control system. A formal procedure for evaluating the responses was prepared with the objective of awarding the contract to the proposer whose proposal best met the requirements

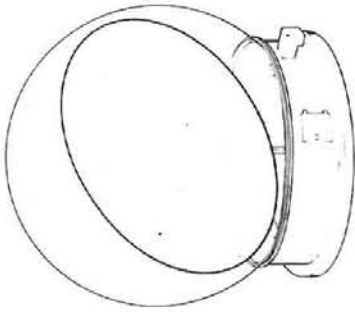
of technical quality, design flexibility, and ease of realignment and focusing as set forth in the RFQ and in a requirements specification document.

These specifications were written primarily to provide flexibility in testing prototype components now being developed for the DOE/Utility-sponsored 10-MWe Pilot Plant under the Central Power Systems Program. Included in the scope of work for the STTF are other applications such as testing components and subsystems of advanced solar thermal systems, high-temperature materials, and photovoltaic panels; using concentrated solar energy for high-temperature chemical and metallurgical processing; and testing and evaluating prototype heliostats.

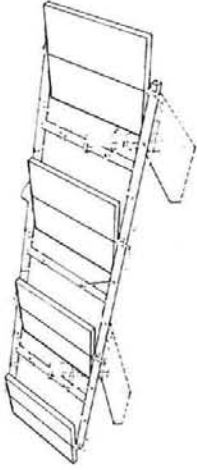
Martin-Marietta was selected to supply the STTF Heliostat Array and Control System on the basis of the evaluation specified above. Items included in the evaluation that addressed technical merit were performance, soundness of design, methods to resolve uncertainties, capability to withstand environments, calibration system, and focusing and alignment system. However, several design features required modification during the fabrication process, as described in ensuing sections.

A two-year development and testing program for the heliostats to be used in the DOE/Utility-sponsored Pilot Plant was conducted concurrent with the STTF heliostat selection. Four contractors built and tested the heliostats shown in Figure 1.

After careful evaluation, the McDonnell Douglas design was selected as the conceptual design for the Pilot-Plant application. With this particular design as the requirement, an RFQ for heliostat detail design was issued that included prototypes for performance evaluation. Responses to this RFQ are being evaluated.

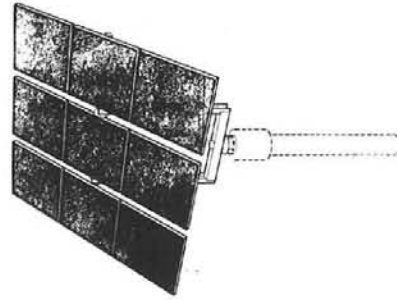


BOEING

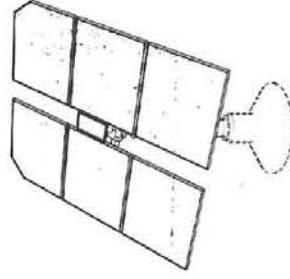


HONEYWELL

HELIOSTATS



MARTIN MARIETTA



MCDONNELL DOUGLAS

PILOT-PLANT HELIOSTATS CONCEPTS
FIGURE 1

STTF HELIOSTAT

The STTF, which uses an array of 222 heliostats in a north field configuration, is capable of supplying 5 MWth energy onto a target on the tower. Data are being gathered from experience with this heliostat array at the STTF, which is currently a primary source of heliostat operational data. The following describes the STTF heliostat system and discusses performance data gathered.

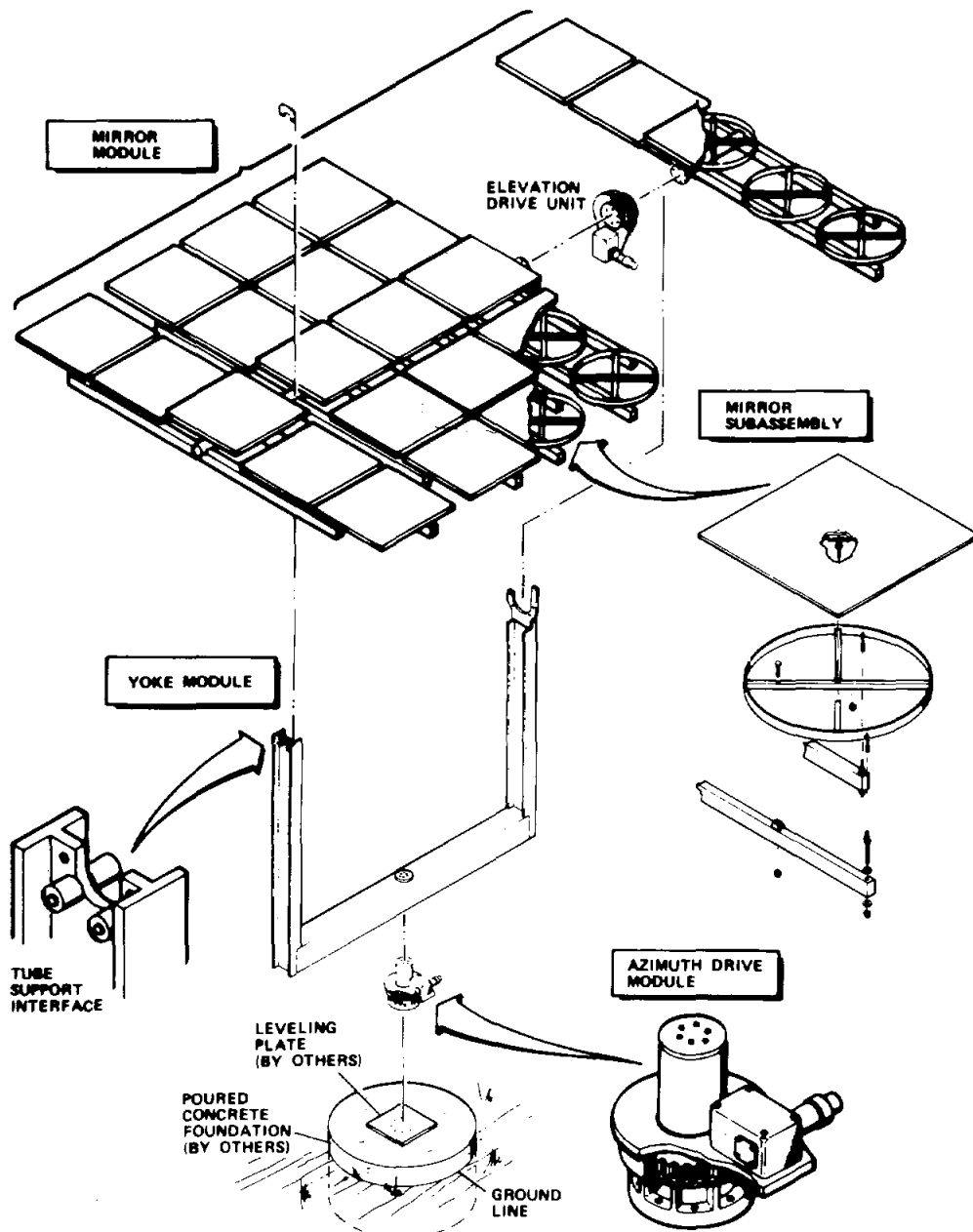
Description

The heliostat system consists of a foundation and azimuth drive, yoke, and mirror modules. The mirror module includes the elevation drive unit as an integral part of the assembly. Figure 2 shows the major components of the Martin-Marietta heliostat.

Figure 3 typifies local conditions at the STTF installation site. The initial foundation design for the heliostats was modified and approved by Sandia Laboratories. Heliostat tracking and pointing requirements limit the foundation tilt to 0.3 mrad under a 13.5-m(30-mph) wind. Load criteria for foundation design are summarized below for a 15.2-m/s(50-mph) uniform wind load.

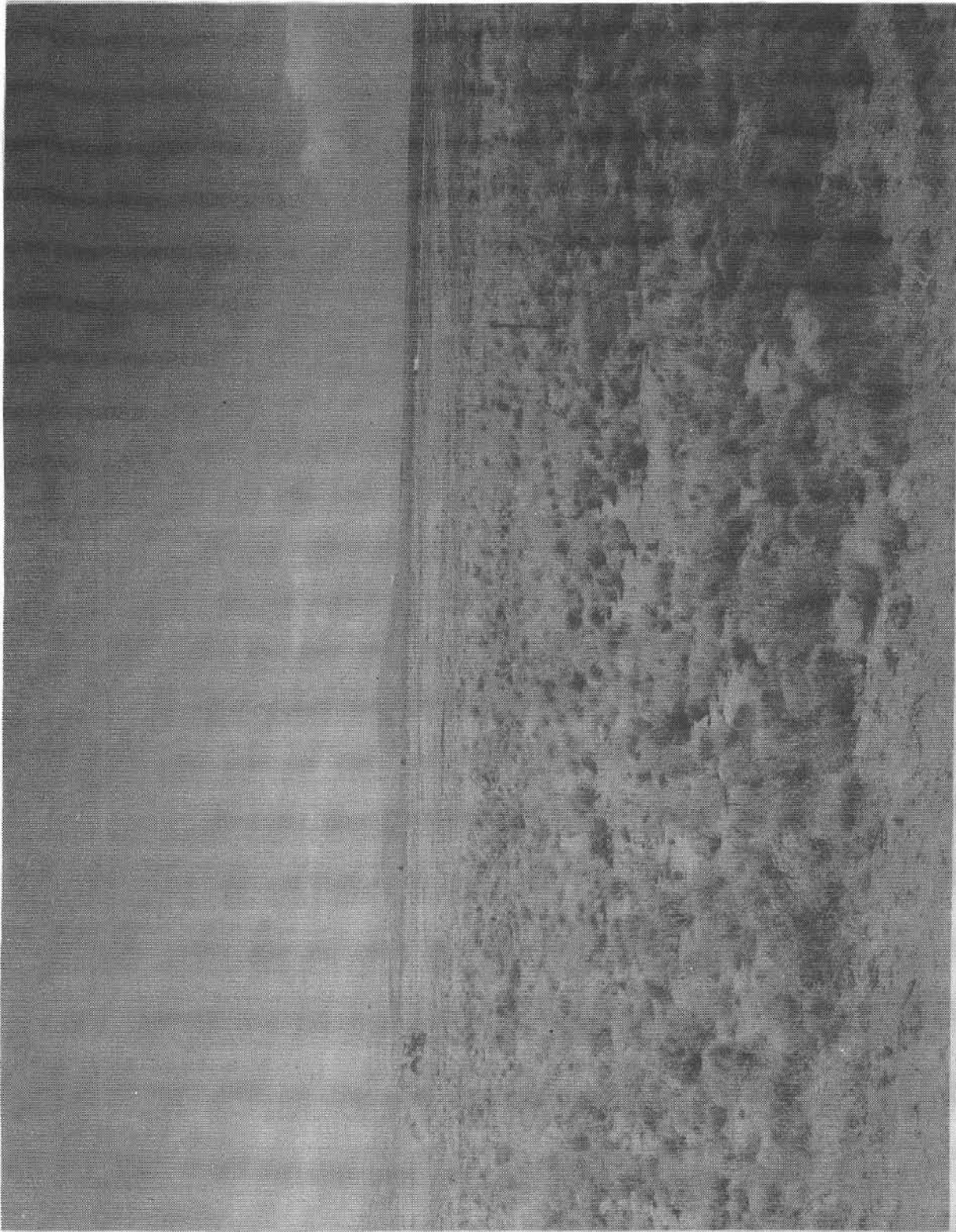
Base bending moment: 53,709 N·m (39,600 lbf-ft)
Base shear: 14,280 N (3210 lbf)
Torque: 6,917 N·m (5100 lbf-ft)
Dead load (axial): 26,690 N (6000 lbf)

Figure 4 shows the poured-in-place foundations (1.2 m high x 3-m base diameter tapered to 1.2 m at the top) using approximately 4.6 m³ of concrete.



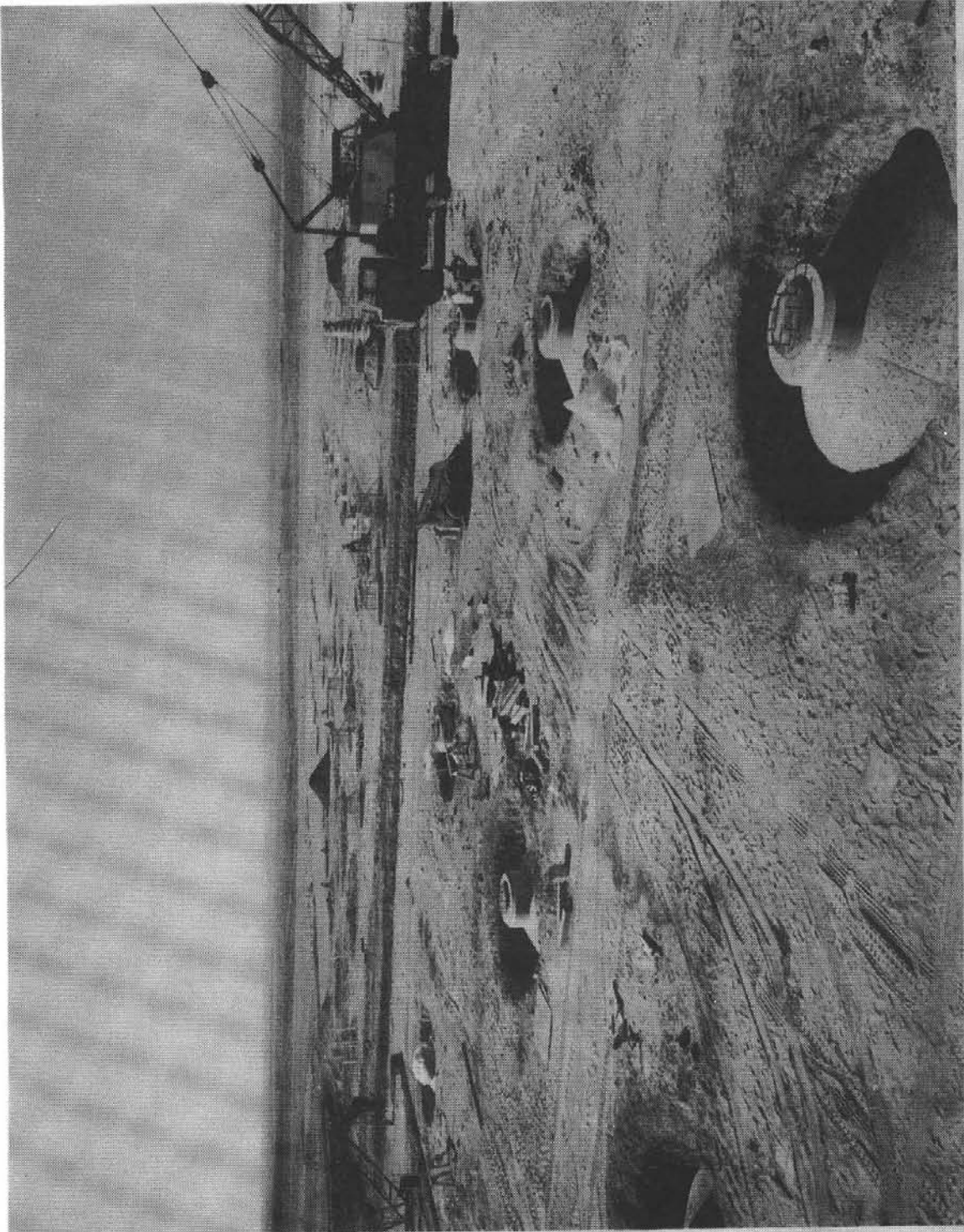
**MARTIN- MARIETTA HELIOSTAT DESIGN
FOR SOLAR THERMAL TEST FACILITY**

FIGURE 2



STTF INSTALLATION SITE

FIGURE 3

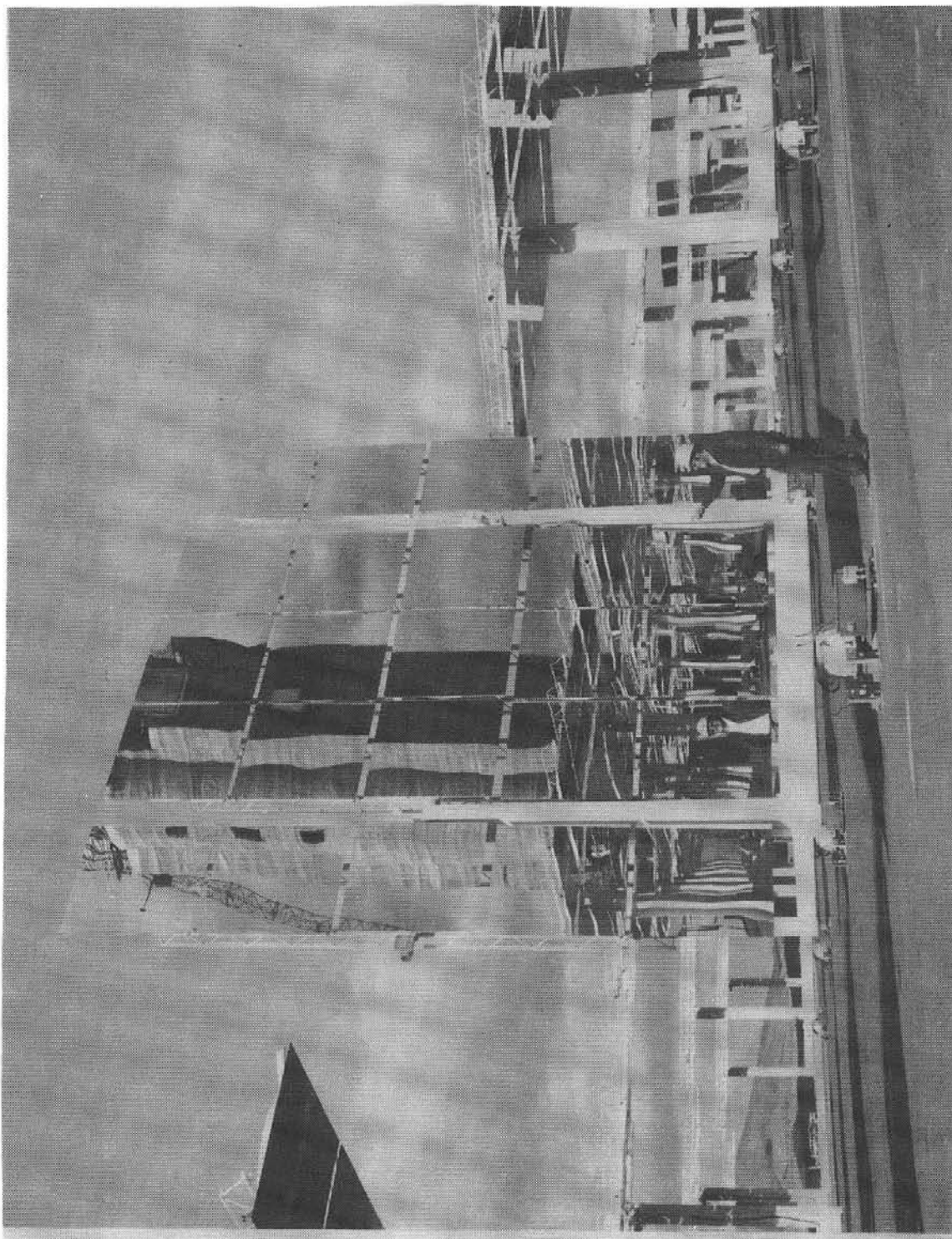


HELIOSTAT FOUNDATION INSTALLATION
FIGURE 4

The mirror module features an array of 25 mechanically distorted mirrors rigidly mounted in a 5x5 symmetrical pattern on gimbaled frames. Each 1.22 m x 1.22 m (4.0 ft x 4.0 ft) square mirror can be individually focused and aligned on its supporting framework. The entire mirror module provides 37.2 m² (400 ft²) of reflective surface and can focus an aberrated image of the sun on a fixed target. Figure 5 shows an STTF heliostat in the vertical or wash position.

An individual mirror assembly consists of a 1.2 m square mirror, a support ring, stabilizer struts, and attachment accessories. The mirror consists of two sheets of 3.2 mm thick double strength float glass, one of which is silvered, and a polyvinyl butyral (PVB) laminate. The silvered sheet has a layer of copper deposited on the silver and is subsequently painted prior to lamination with the second sheet of float glass.

Each mirror requires a separate warping structure to achieve proper focusing. This technique is based on providing local stiffening in the form of a 1.17-m(46 in.)-diameter steel hoop centered on the mirror and mounted on the back. This hoop, which is securely bonded to the back of the mirror with an elastic bonding agent that remains flexible over wide extremes in temperature, is reinforced by a planar strut assembly composed of two square tubes welded to the hoop. These tubes intersect at the hoop/mirror centerline to form a cross structure oriented along the mirror diagonals, and provide pickup and attachment points for the mirror. Pads with integral threaded studs are bonded to the mirror at the centerline. The "cross" structure, in conjunction with the hoop stiffener, provides the reaction structure with which the mirror can be warped. The hoop frame becomes the edge support that allows the mirror to act as a simply supported plate free to rotate in circular symmetry. Warping forces are applied at the mirror centerline through the threaded stud fastener and jamb nuts and at the corners by corner-push studs.



STTF HELIOSTAT IN VERTICAL POSITION
FIGURE 5

The azimuth drive module incorporates the azimuth drive mechanism (which includes an optical position encoder with 2^{13} address locations), azimuth bearing system, and a mounting flange for securing the entire heliostat assembly to the foundation. This module, the first component of the heliostat assembly to be installed in the field, is lowered over a ring of threaded anchor studs embedded in the foundation. These studs protrude through a leveling plate that provides a stable mounting base. The yoke module is lowered by crane and attached to the azimuth drive module. The last item to be installed is the mirror module.

Heliostat drive systems are capable of maneuvering the heliostat as follows:

- 1) Azimuth, $\pm 2.40 \pm 0.44$ rad ($\pm 137.5 \pm 2.5$ deg);
- 2) Elevation, $04.71 \begin{smallmatrix} +0.00 \\ -0.09 \end{smallmatrix}$ rad ($-270 \begin{smallmatrix} +0 \\ -5 \end{smallmatrix}$ deg);
- 3) Azimuth slew rate, 13.4 rad/h (755 deg/h);
- 4) Azimuth tracking rate, 1.5 rad/h (89 deg/h);
- 5) Elevation slew rate, 17.82 rad/h (1133 deg/h);
- 6) Elevation tracking rate, 0.84 rad/h (48 deg/h).

The yoke module, the major structural element in the heliostat assembly, transfers wind-induced loads directly to the azimuth bearings. The vertical members of the yoke module are fabricated from wide flange sections welded to a horizontal member fabricated from square commercial tubing. At the center of the square tube section, corresponding to the azimuth center of rotation, a welded steel tube section provides for centering registration of the yoke module on the stub shaft of the azimuth drive module. After the yoke module has been lowered into position, centered, and properly seated on the azimuth module, the threaded studs are torqued to provide a rigid, self-centering connection to the azimuth drive unit.

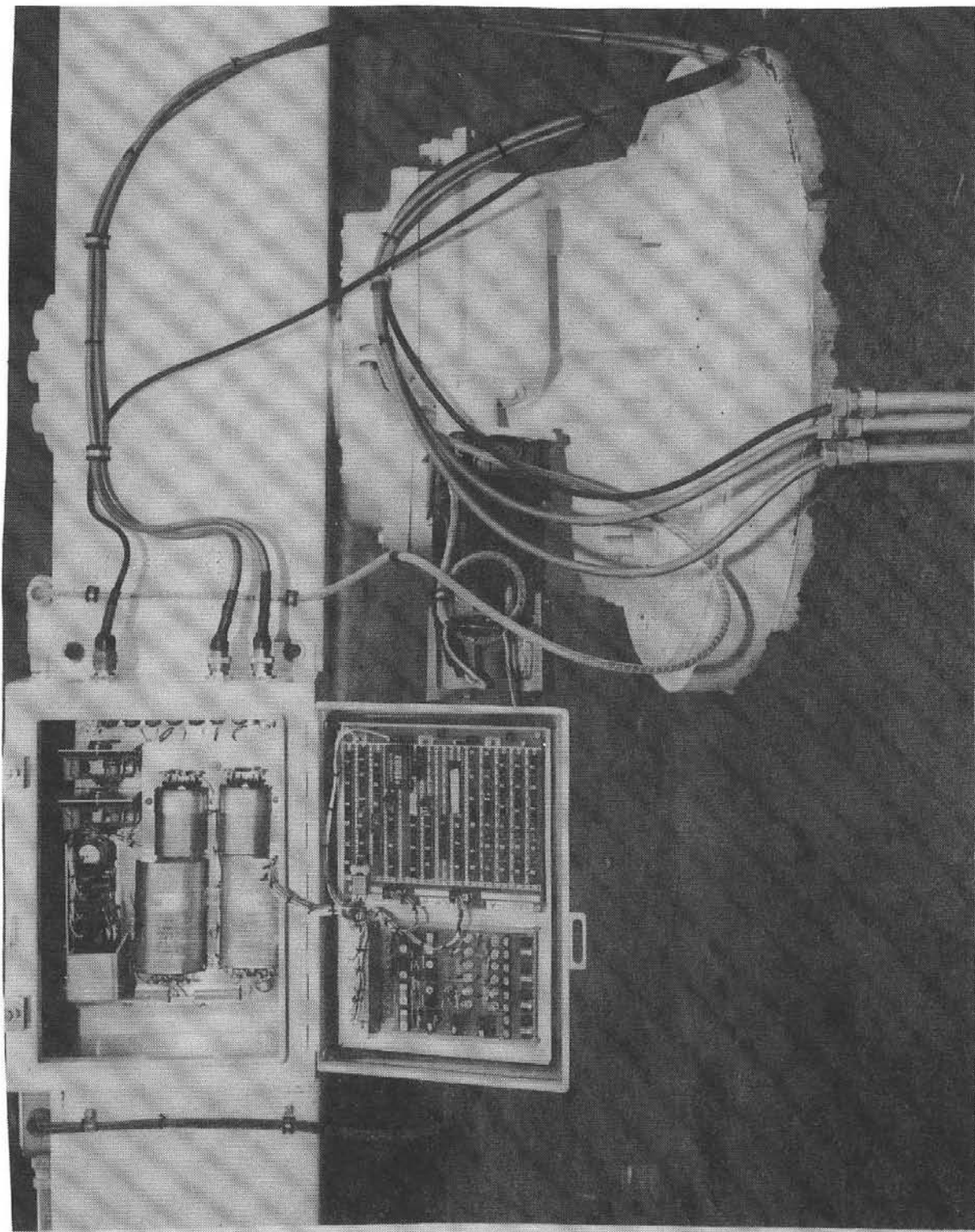
In its normal tracking mode, the heliostat is capable of continuously tracking the sun while maintaining pointing control to ± 1.5 mrad in wind velocities up to 13.5 m/s (30 mph). At higher velocities the heliostat will be returned to the face-down stowed position. Structurally, the heliostat can survive the effects of sustained wind velocities of 32 m/s (71.6 mph) with gusts up to 44.7 m/s (100 mph) without permanent deformation or mechanical degradation.

A Heliostat Control Electronics (HCE) is located on each heliostat and interfaces with the Heliostat Array Control (HAC) through a Heliostat Interface Module (HIM). The HCE performs all functions necessary to control the heliostats in the slew and track modes. The electronics contain interface isolation, data check circuits, position comparators, motor drivers, and output data formatting and processing logic. Figure 6 shows an open HCE mounted on a heliostat.

The HCE is housed in a sealed enclosure on the lower heliostat yoke. Control electronics circuits are packaged on a separable subchassis together with power supplies mounted within its lower compartments. Two printed-circuit-board assemblies are (in the basic configuration) located along the top surface of the subchassis and interconnected by an internal wiring harness.

The housing is designed to prevent moisture, sand, or dust intrusion. Access to the electronics is provided by a removable cover secured with captive fasteners. Sealing washers are used in conjunction with the fasteners for a weatherproof seal.

The HCE has the capability for 16 operation modes. Currently 14 specific functions are defined. The following list categorizes the functions into 6 classes:



HELIOSTAT CONTROL ELECTRONICS UNIT

FIGURE 6

- 1) Status - HCE status returned to HAC.
- 2) Clear - All HCE mode registers are cleared and all motors stopped.
- 3) Coarse track - Slew motor of specified axis is activated in closed-loop operation (one azimuth command, one elevation command).
- 4) Fine-track - Track motor of specified axis is activated (one azimuth command, one elevation command).
- 5) Direct stow - Four commands allow specified axis track motor to be activated in either clockwise or counter-clockwise direction. Only limit switches or clear command will turn the motor off.
- 6) Direct slew - Four commands allow specified axis slew motors to be activated in either clockwise or counter-clockwise direction. Only limit switches or clear command will turn the motor off.

To assure safe operation of the heliostats for both personnel and equipment, the following features are incorporated in the design

- 1) Pointing limits - HAC control programs preclude pointing the reflected beam of any heliostat toward any position located out of a preselected region.
- 2) Limit switches - Limit switches are located at each end of azimuth and elevation travel of the heliostat axis. These are provided to avoid twisting ground straps and associated cabling.
- 3) Manual Control Box - Local control of the heliostat is possible only when this box is connected to the HCE unit. When it is connected, HAC control of the heliostat can be locked out.

Focus and Alignment

Focusing of STTF heliostat facets is accomplished by first dividing the heliostat field into seven focusing zones. The

facets are focused during assembly to correspond to the focal zone in which they are installed.

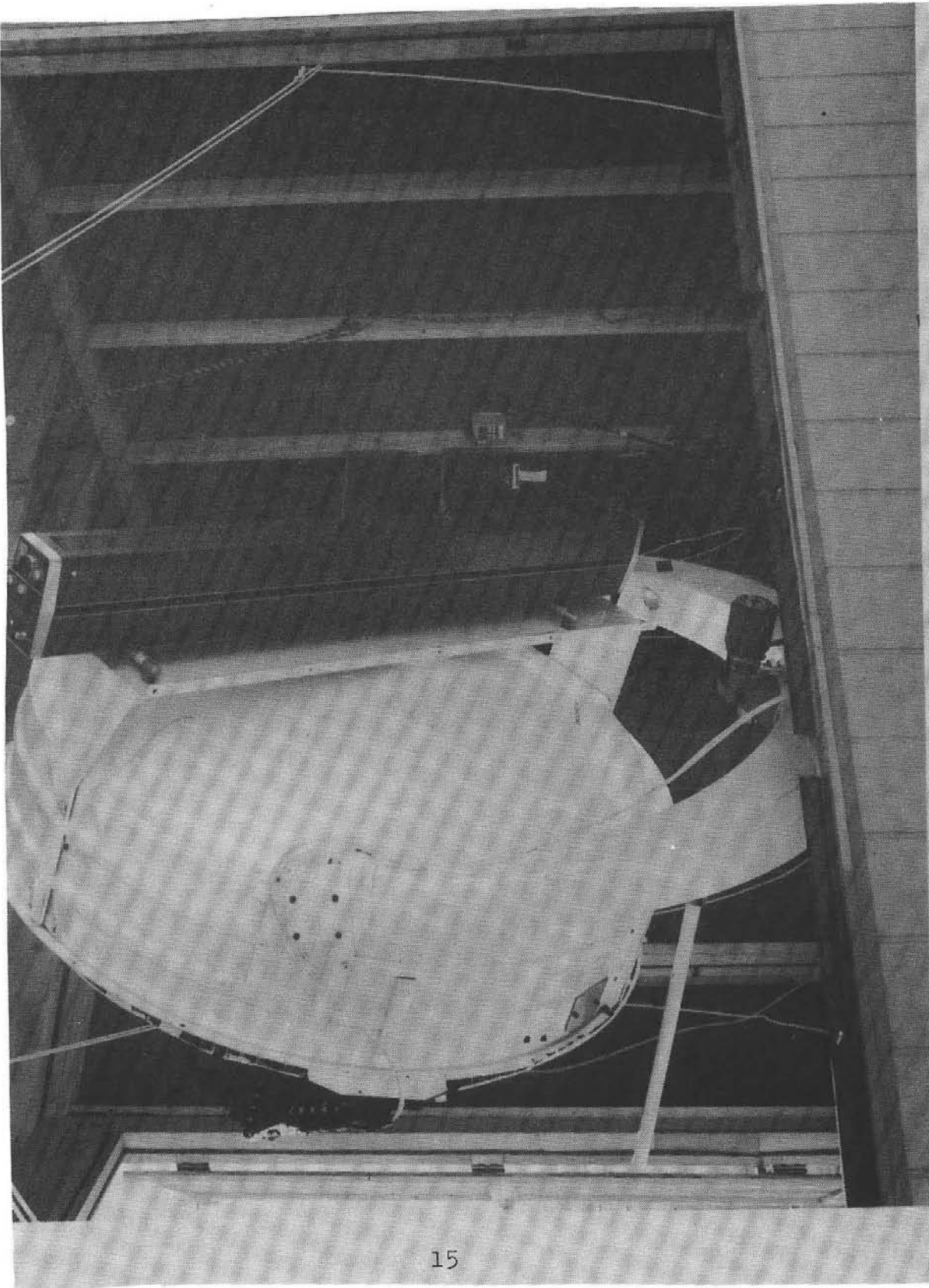
The alignment subsystem consists of a laser collimator (L/C) (shown in Figure 7), control and monitoring equipment at the heliostat, and a display target.

The beam from the L/C is approximately the size of the 1.2 m square mirror facet. The control system is used to position the heliostat so that the laser reflection from the center facet is displayed on the center of the target. The heliostat position is noted and encoder biases are recorded. For the remaining 24 facets, the heliostat is oriented, and the L/C is repositioned by the computer to form the proper geometry. Each facet is subsequently aligned to reflect the laser beam to the target center. Figure 8 shows this alignment activity.

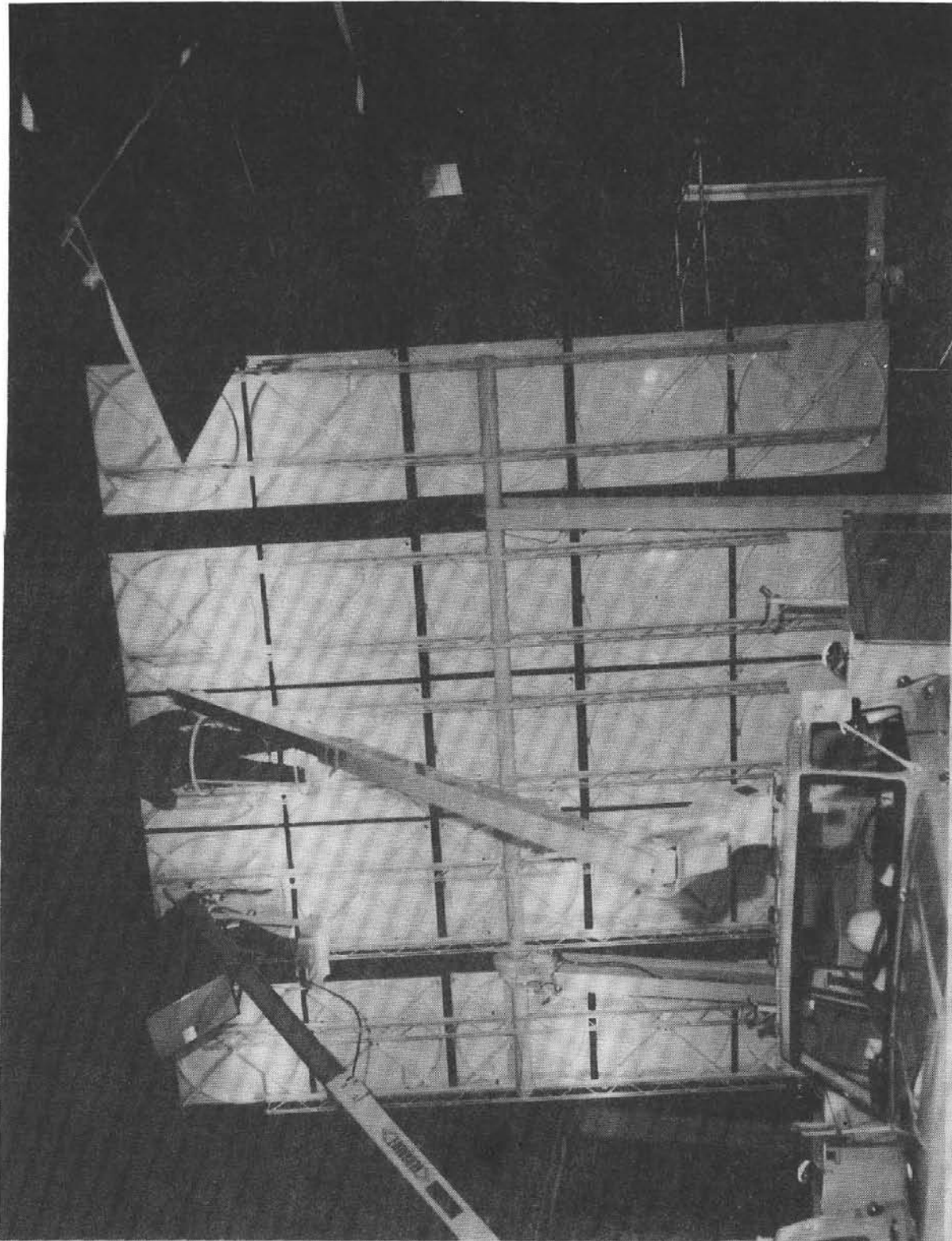
Control

The heliostat pointing commands from a preprogrammed test sequence or from the facility operator are analyzed by the Master Control System (MCS) and distributed to the heliostats for execution. Heliostat Array Controllers (HAC) communicate with up to 128 heliostats in their jurisdiction. Each HAC sends MCS generated commands, and HAC generated azimuth and elevation pointing information to its four associated Heliostat Interface Modules (HIM) to be transmitted to the appropriate heliostats. Each heliostat receives an aiming vector update once every second and responds with its own status. The HACs also process alarm messages such as tracking or communication errors.

The commands and data transmitted to the individual heliostats are received and executed by the Heliostat Control Electronics (HEC). The HCE provides power to the drive motors until the position encoders indicate that the appropriate heliostat



STTF LASER COLLIMATOR ALIGNMENT SYSTEM
FIGURE 7



SSTF ALIGNMENT ACTIVITY

FIGURE 8

attitude has been attained. The HCE and heliostat motors then await the next command.

Figure 9 shows the facility operator console with video displays. Figure 10 shows a closeup of the heliostat field status display with the information available to the facility operator.

Design Modifications Made During Fabrication

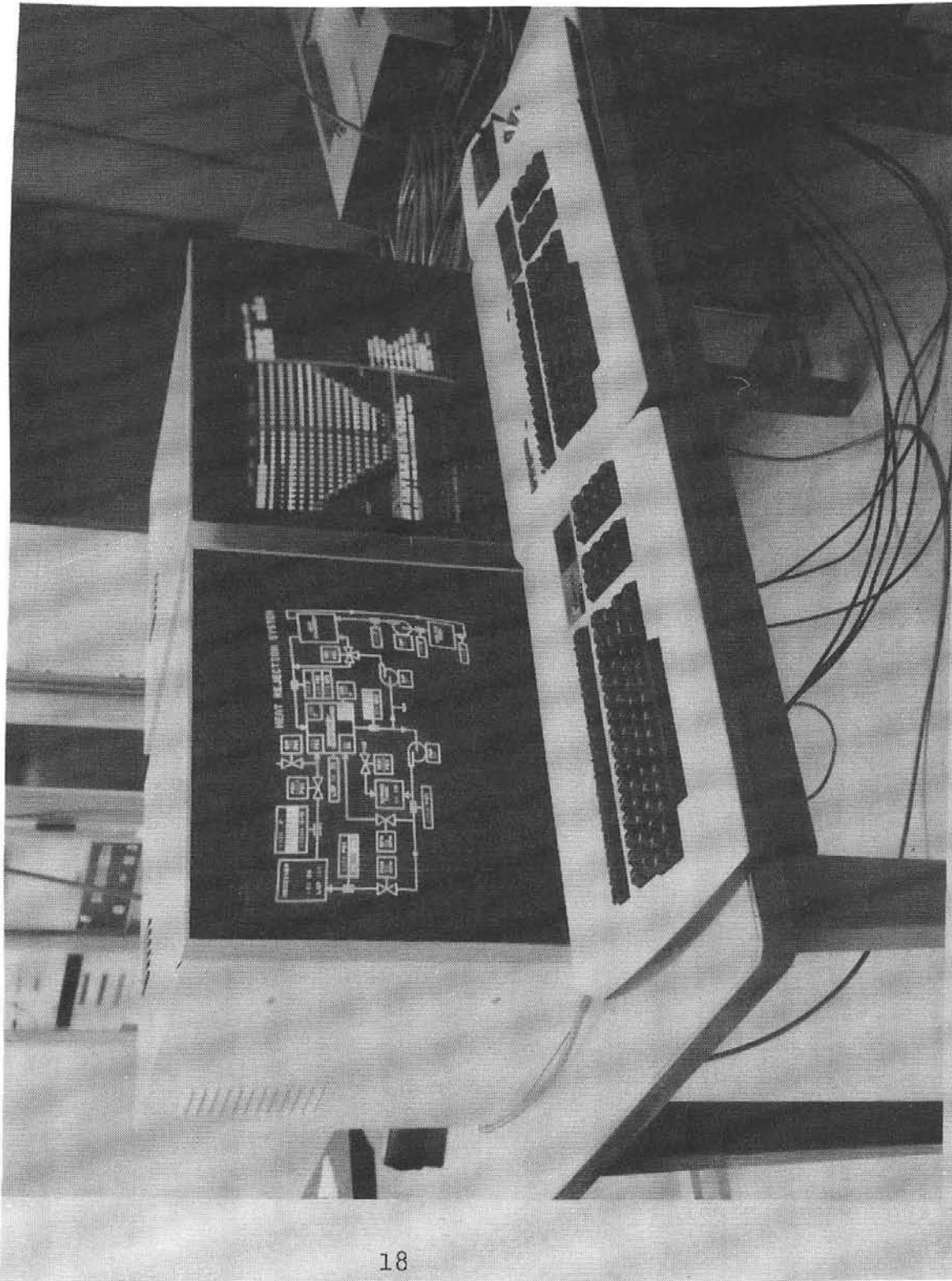
Several design features required modification during heliostat fabrication to provide acceptable operation, as follows:

1. The original design proposed the use of low-iron drawn glass bonded to a back sheet of float glass to achieve higher reflectivity. Mirror cracking due to internal and thermal stresses, and marginal optical performance required a change to all-float glass laminated mirrors.
2. The original mirror module steel support structure proved too weak for stable mirror support; a stiffer structure with added mechanical deformation features ("corner pushers") was substituted.
3. Focussing of each mirror was originally intended to be done with the laser collimator tool after field installation. Use of a mechanical surface gage to set facet curvature in the factory was devised.
4. The elevation and aximuth mechanical gear boxes were fitted with additional environmental seals and with a drive gear backlash adjustment feature to improve tracking accuracy.

HELIOSTAT PERFORMANCE

Maintenance and Repair

The STTF has only recently become operational; however, nighttime heliostat operation activities were conducted for



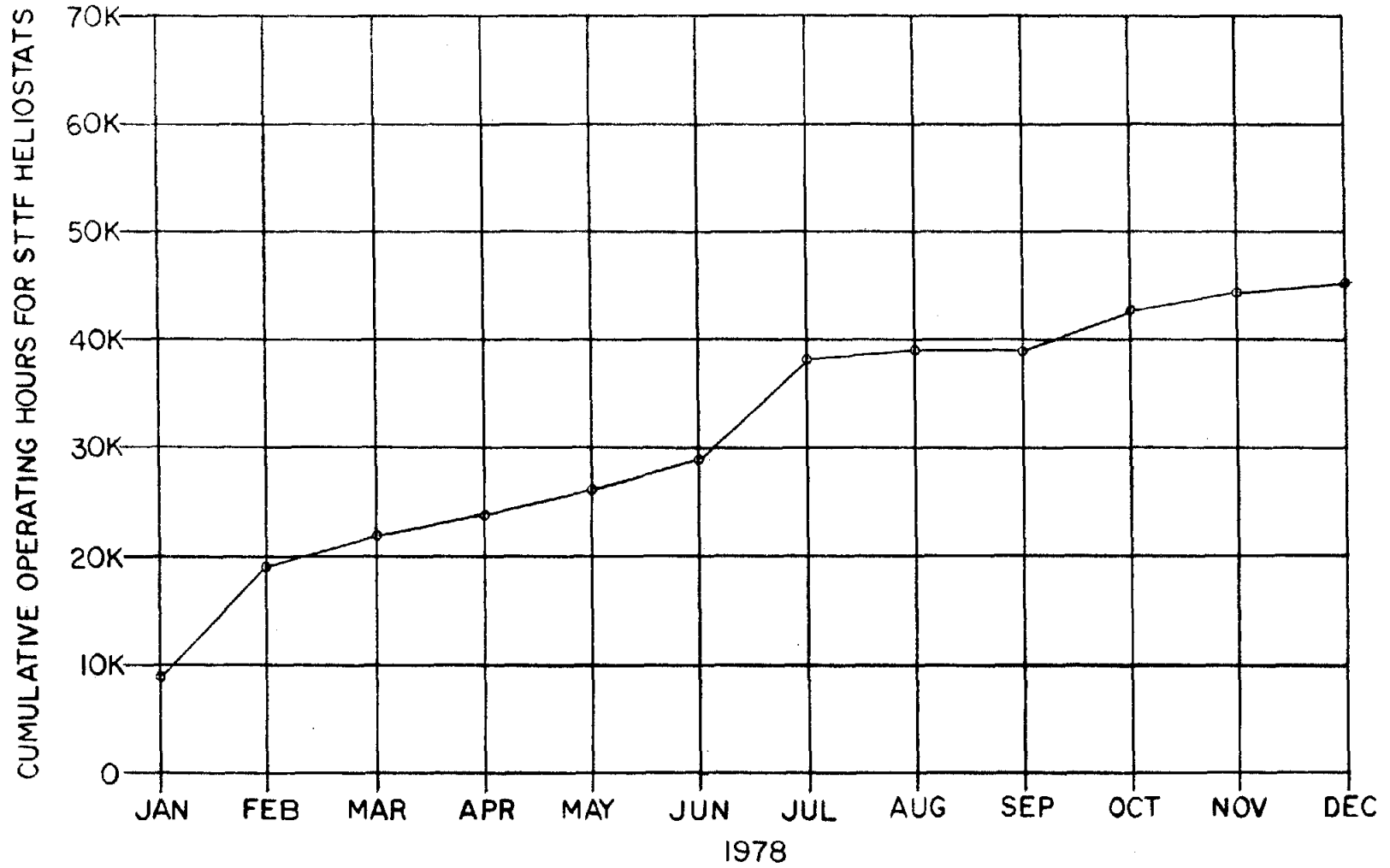
STTF CONTROL ROOM OPERATOR CONSOLE

FIGURE 9

approximately eight months during the construction phase. The purpose of these operations was to obtain experience with failure mechanisms and to incur any inherent infant mortality in the heliostat hardware. Figure 11 is a graph of the cumulative STTF heliostat hours of operation to date and Figure 12 presents the STTF field status as a percent of operational heliostat versus time.

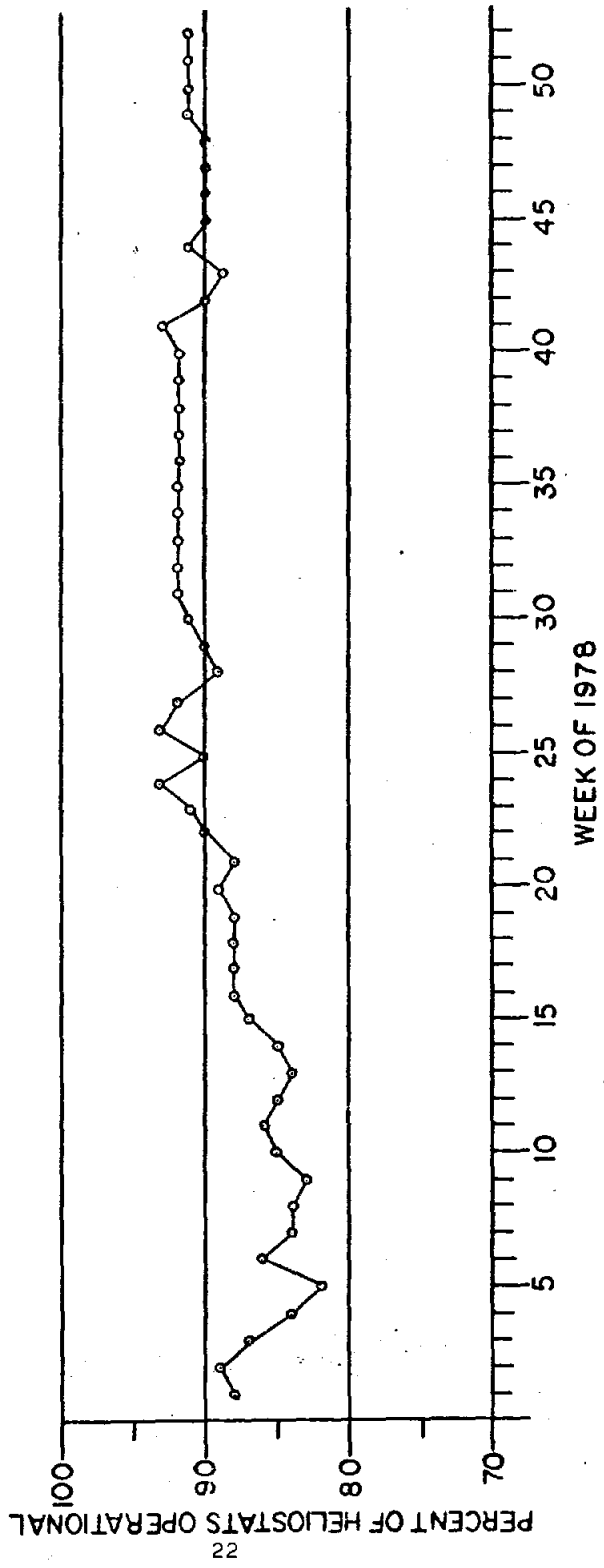
The types of failures that have been encountered fall into the following categories: 30% Drive Mechanisms (Azimuth and Elevation); 30% Heliostat Control Electronics; 30% Intermittent; and 10% Other. Azimuth and elevation drive failures have been primarily related to optical encoder failures. Most encoder failures are due to an adjustment fault in the encoder alignment and have been corrected on heliostats that have failed. The HCE problems involve electrical component failures. Most components used are commercial grade. A relatively large number of intermittent failures have been encountered. These failures are seasonal (i.e., larger percentage in colder months), which suggests a temperature dependence. More data will be required to identify the nature of these failures. Other failures have been identified as design deficiencies and suggest areas requiring engineering attention. For example, inadequate sealing problems and connector problems have been identified. Moisture and resulting rust on the metal surfaces have been found in almost all heliostats that have failed. This problem is being addressed. Correction of these and similar problems and a continued decrease in failures due to infant mortality should improve the field operational status to 95%. (These data are for STTF heliostats only and cannot be directly translated to other types of heliostats.)

During this period, an average crew of four workers has been assigned to heliostat repair. Clearly this level of O & M is not acceptable for practical central receiver plants, and further development of reliable electrical and mechanical systems is required.



CUMULATIVE STTF HELIOSTAT HOURS

FIGURE 11



STTF HELIOSTAT FIELD STATUS

FIGURE 12

Reflectivity

The STTF reflectivity program has been initiated to measure losses in mirror reflectance due to environmental influences.

Since it was necessary to detect small changes in reflectivity, an accurate technique for reflectivity measurements was required. A technique described in a forthcoming publication entitled Specular Reflectance Loss of Solar Mirrors Due to Dust Accumulation by R. B. Pettit, J. B. Freese, and D. E. Arvizu of Sandia Laboratories was adopted. This technique uses a bidirectional reflectometer that allows investigation of both wavelength dependence and surface specularity. Preliminary testing on STTF mirror samples indicated that a simplified measurement technique could be used to characterize solar average reflectance at a sample location. This measurement technique includes reflectivity measurements at only one or two wave-lengths per sample location and this greatly reduces the number of measurements required. This program includes 54 15.2-cm(6-in)-square flat mirror samples mounted on heliostats and distributed throughout the STTF field (see Figure 13).

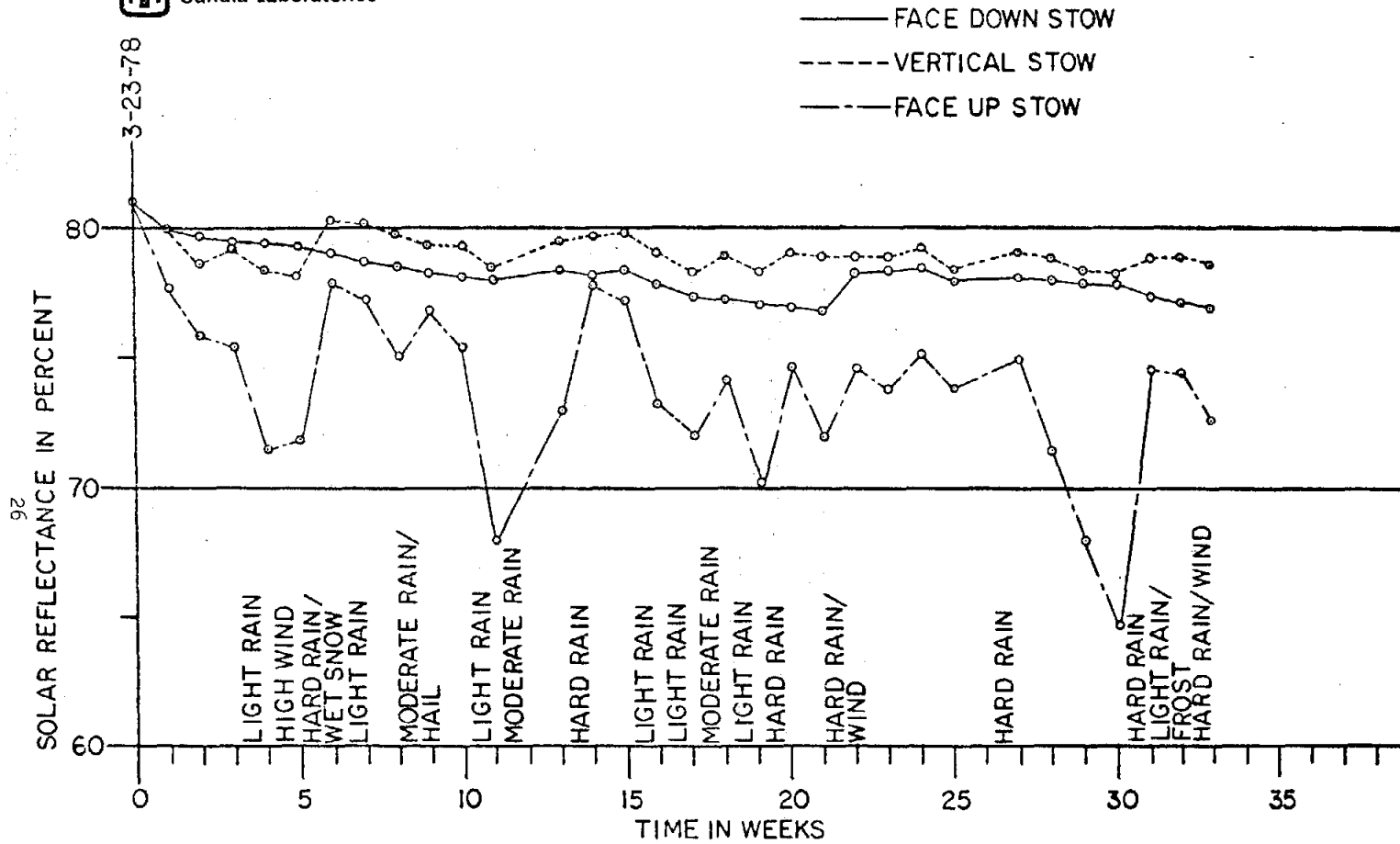
Some work on the statistical requirements to characterize mirrors has been done. For one STTF mirror sample the statistical requirements (number of random locations necessary) to characterize the mirror surface based on measured reflectivity variances and specific source beam diameters of 0.66, 1.23, and 1.93 cm were found to be 21, 17, and 14, respectively. This work was done by R. B. Pettit, J. B. Freese, and C. R. Clark of Sandia. Parameters to be investigated in the STTF reflectivity program include reflectivity degradation as a function of time, field location, and stowage orientation; and influences on reflectivity from natural cleaning phenomena, cleaning agents, and wash/rinse procedures.

INSTRUMENTATION MIRROR MOUNTED ON HELIOSTAT FRAME

FIGURE . 13

A significant amount of work is necessary to develop optimal cleaning procedures. However, in the interest of acquiring data and developing experience with a specific technique, it was decided to commit initially to a high pressure water/detergent application technique. This decision was based on testing done at the STTF where mirror samples were cleaned using a 300-psi and 3-gpm water stream with several detergents and solvents. This testing indicated that with a high pressure application technique it was possible to recover from 80 to 90% of the reflectance loss caused by short term environmental influences. During testing conducted by Sandia Labs personnel at Tritan Corporation of Houston, Texas, (contracted by STTF to build and deliver a mirror washing vehicle) some dirty mirror samples were subjected to 500-, 1500-, and 10,000-psi tap water streams. Reflectivity tests showed no significant differences in recovered losses with these three pressures. All recovered about 95% of the original 0.81 average solar reflectance.

Figure 14 shows the influence on average solar reflectance of stowage orientation with time. These data show that a horizontal "face-down" stowage is not as influenced by environmental conditions as the vertical "face-south" or the horizontal "face-up" stowage orientation. Observation of the change in reflectance values, measured after moderate to hard rains, supports the logical assumption that in the vertical or the "face-up" stowage orientation rain can be useful in cleaning mirrors. However, light rains, especially when combined with blowing dust, can also have undesirable results in the orientations mentioned. The "face-down" stowage is surprisingly free of the environmental conditions noted. In this testing the mirror samples remained in their respective stowage orientation when the field heliostats are stowed and move correspondingly when the heliostats are moved. This should be considered in extrapolation of the data to address operations which place heliostats in many orientations during a 24-hour period. One additional observation is that



REFLECTANCE VS. TIME
 FOR
 DIFFERENT STORAGE ORIENTATIONS
 IN STTF HELIOSTAT FIELD
 FIGURE 14

environmental influence on mirror surfaces can occur in time periods as short as a few minutes

Beam Characterization System

As part of the STTF heliostat evaluation program, a Beam Characterization System (BCS) is under development. Several alternatives have been and continue to be investigated. Current work specifically addresses evaluation of the 10MW_e Pilot Plant heliostat prototypes.

As a measurement of beam "quality," the BCS will verify that a heliostat can concentrate reflected energy within a specified area. This will be accomplished by first calculating the theoretical beam shape for the given geometry and test conditions using the Sandia provided HELIOS program. This theoretical beam shape will then be compared to the measured beam shape data obtained with the BCS.

The proposed BCS technique is a refined version of a widely used video camera-based thermal or radiometric imaging system that is complemented with a video digitizer and a computer interface. Necessary refinements involve (1) the techniques used in calibrating video gray scale levels, (2) the determination of the relation between video output level and the actual heat-flux density incident on the target, and (3) arriving at a spatial calibration to relate the distance between digitized scan lines to the corresponding distance on the beam target. Once the digitized array of data has been determined using appropriate calibration techniques, the data can then be manipulated in an associated computer system to give the following outputs: 3-D flux density plots, total power level, beam centroid location, pointing and tracking accuracy determination, and power within a given radius from the centroid.

This technique is versatile and potentially highly accurate and precise. Advantages include a wide range of target intensity measuring capability (accomplished by adding appropriate neutral density filters to the camera), possible use of the system as a heliostat alignment tool, and possible use for infrared scanning of receivers as a check for hot spots.

A second technique under study is a photographic technique using appropriately selected film that can be digitized in a manner similar to the video generated data using a photodensitometer. One limitation of this technique is its inability to process data in real time.

A third alternative for a BCS involves the use of circular foil heat flux gages. Since cost, calibration, and maintenance of a two-dimensional array of gages are untenable, an instrumented sweeping bar technique has been investigated. To demonstrate this technique the STTF designed a Cal-bar system that measures single heliostat flux density profiles. Since this measurement hardware requires the use of a ground target, constraints are introduced in the heliostat orientations to be tested.

The measurement procedure involves either sweeping the instrumented bar horizontally across a beam projected onto a ground target or sweeping the beam across a stationary bar. The instrumented bar is approximately 5-m long and can accommodate 64 gages spaced at 7.6-cm(3-in) intervals. The bar is water-cooled to keep the gages within their specified operating temperature range during measurements.

The heat flux gages used are the circular foil type covered with a quartz window. Their ranges are 0.1 W/cm^2 and 0.2 W/cm^2 full scale with linear response over the entire spectral and thermal range, and they have a nominal response time of 250 ms.

Beam Measurements

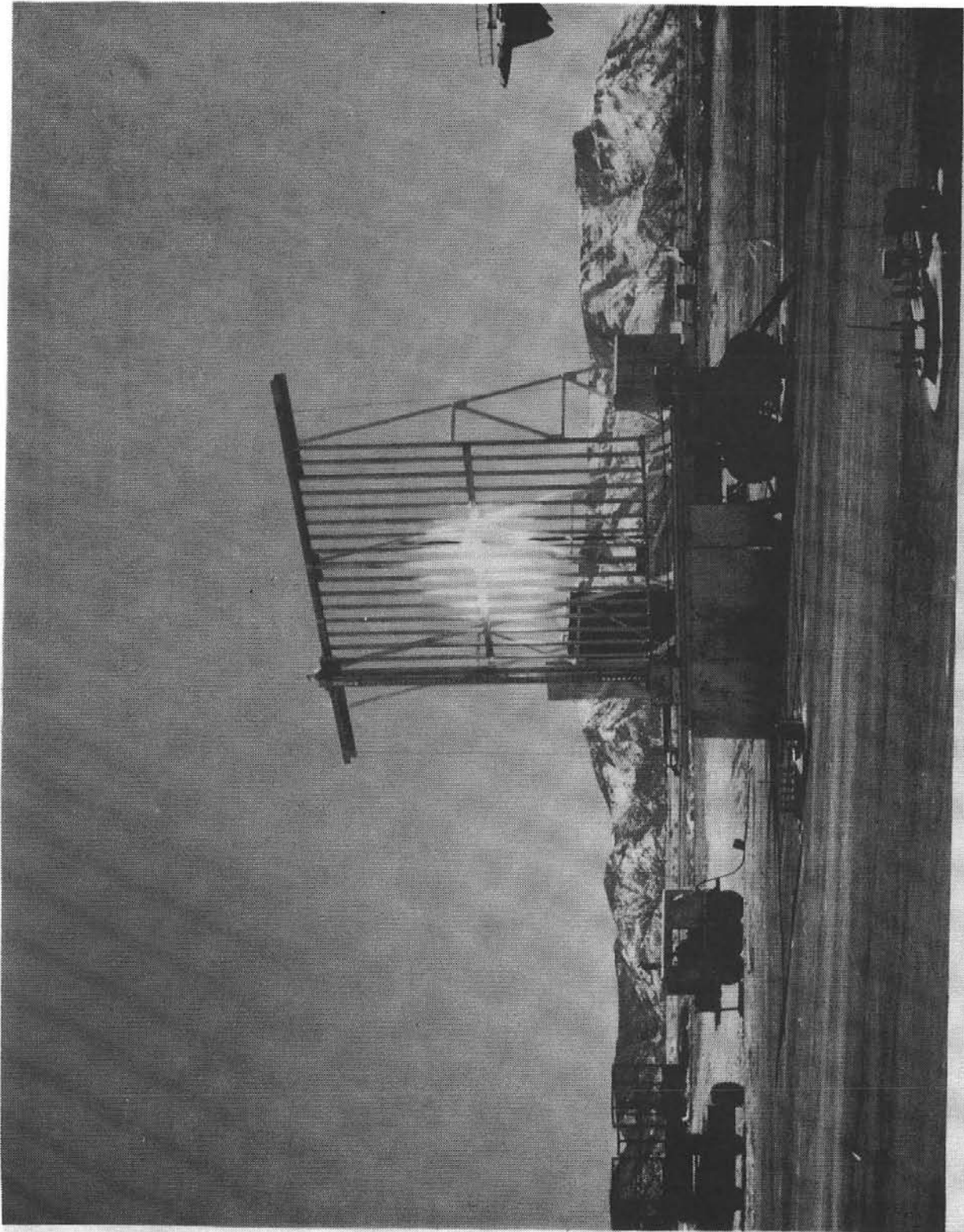
Several tests using the Cal-bar have been conducted on facility heliostats. In these tests, heliostat beams were swept across the bar to eliminate tracking influences. Figure 15 shows the Cal-bar in position with a heliostat beam just prior to sweep.

A series of six tests was run. Three heliostats, selected along the northeast edge of the field, were measured with alignment conditions both matched and mismatched to the run conditions (i.e., aligned for day 70 measured on day 77 and aligned for day 344 measured on day 56.)

Comparison of these figures shows only minor (a few percent at most) improvements of reflected energy into a specified area, primarily a 12-mrad circle, from the matched alignment conditions to the mismatched alignment conditions. One heliostat was measured before and after cleaning. No difference was detected; however, a heavy thunderstorm had "naturally cleaned" the test heliostats which were stowed in the vertical wash position before testing the uncleaned condition.

Some of the asymmetry of the observed beam shape can be accounted for as measurement error. A gage on which the zero-level needed adjusting was identified after the test. Since the measurement system accuracy is 5 to 10%, including the changing environmental conditions during the 20-second bar sweep, data manipulation was not undertaken. Results of these tests tend to be more useful as a qualitative rather than quantitative measure of heliostat performance.

The following table gives specifics of the tests that were conducted:



CAL-BAR BEAM MEASUREMENT SYSTEM

FIGURE 15

TABLE I

HELIOSTAT ALIGNMENT CONDITIONS FOR CAL-BAR TESTS

<u>Field</u> <u>Location</u>	<u>Slant Range</u> <u>(Meters)</u>	<u>Test No.</u>	<u>Conditions</u>		
			<u>Align</u> <u>Day</u>	<u>Test</u> <u>Day</u>	<u>Insol.</u> <u>(W/cm²)</u>
7N9E	128	119/7	344	56	.105
7N9E	128	119/A	70	77	.107
9N11E	156	108/4	344	56	.104
9N11E	156	108/7	70	77	.108
11N13E	190	79/3	344	56	.103
11N13E	190	79/5	70	77	.107

Figures 16, 17, 18, 19, 20, and 21 show the measured data from tests 119/7, 119/A, 108/4, 108/7, 79/3, and 79/5, respectively. These figures show (1) the percent of incident power collected vs. beam radius from energy centroid, and (2) a two-dimensional contour plot of the beam shape, where the cross hair indicates the centroid and the isoflux density (constant flux) lines are 90, 70, 30, and 10% of the measured peak flux density value. The dotted line indicates the 12-mrad circle for the given slant range.

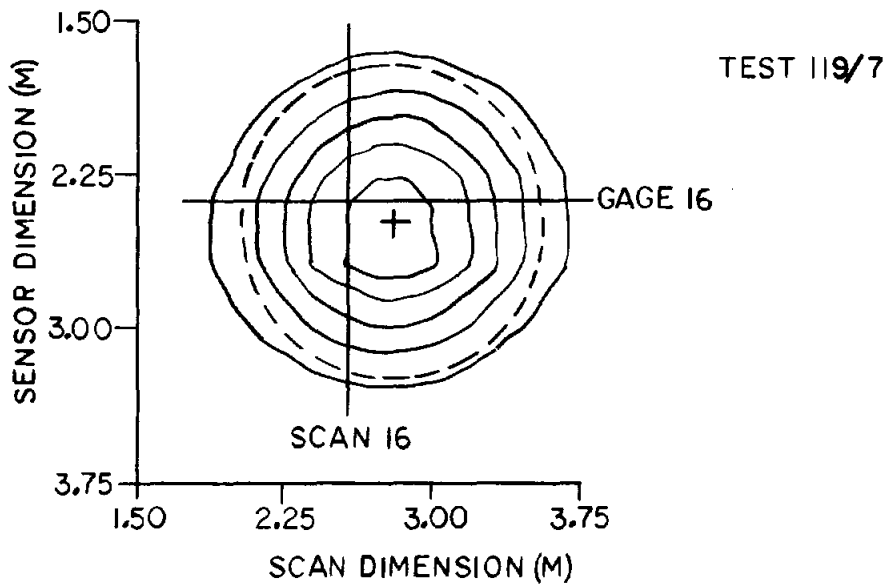
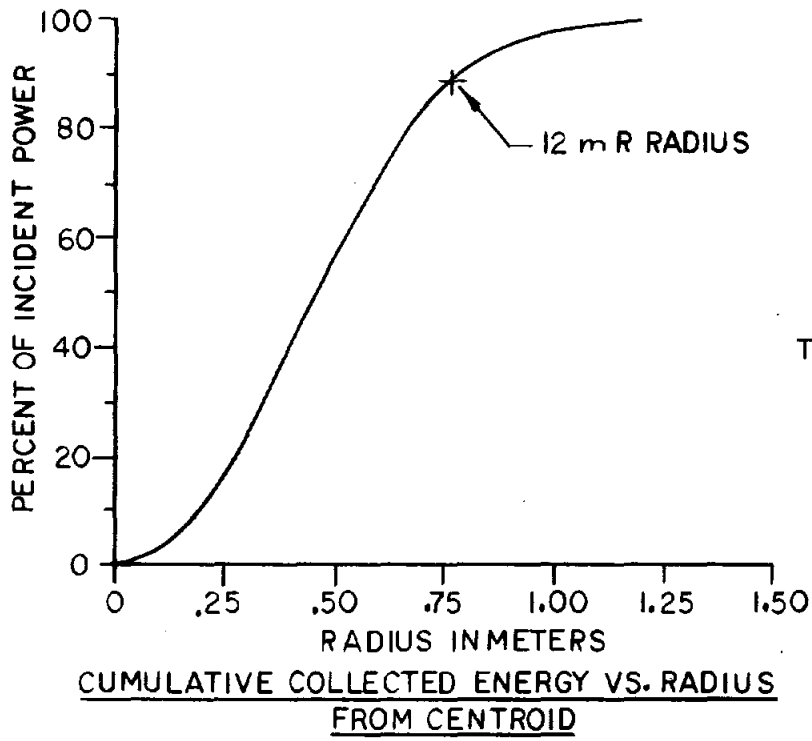


FIGURE 16
CONTOUR PLOT

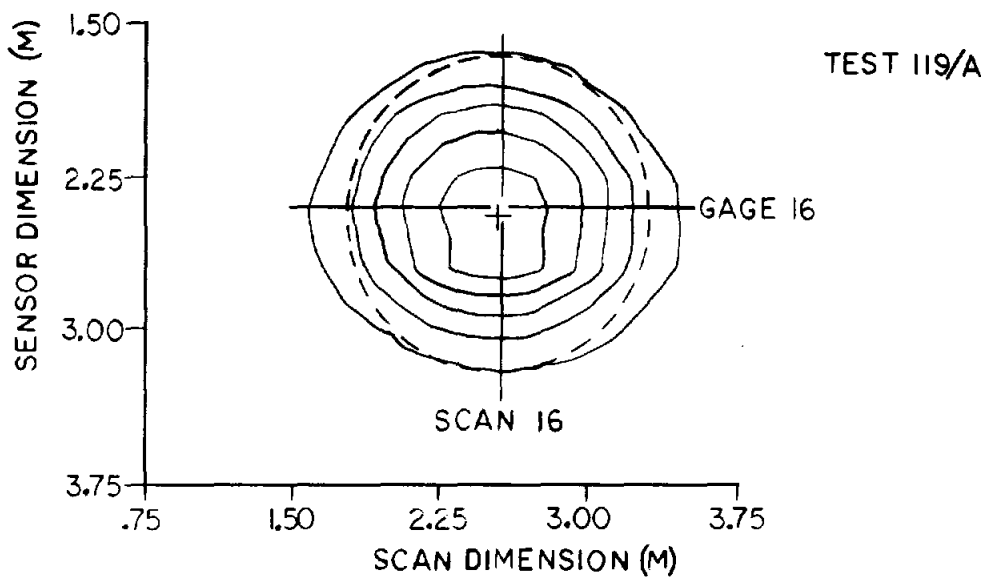
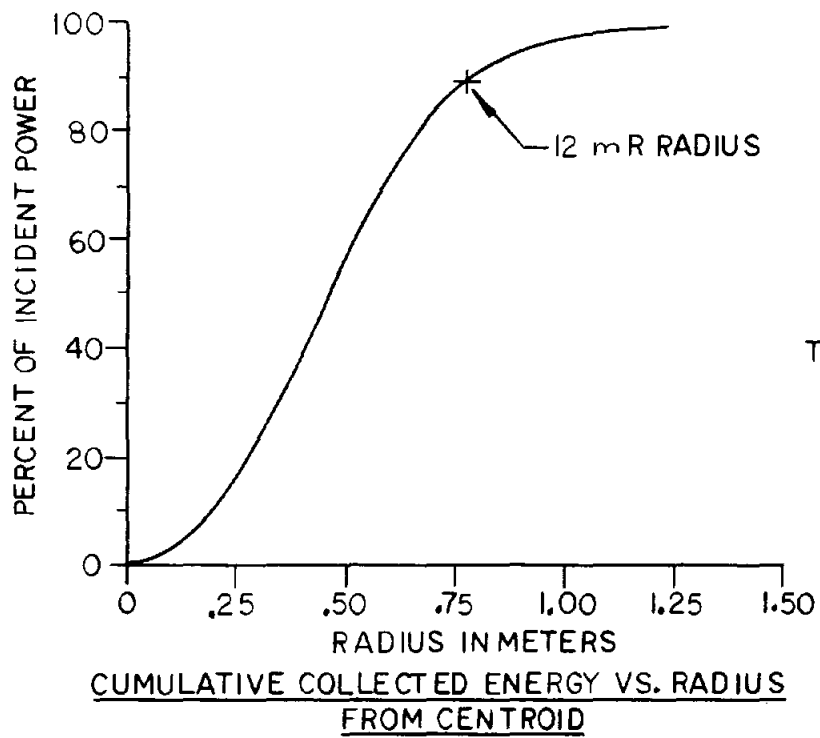


FIGURE 17
CONTOUR PLOT

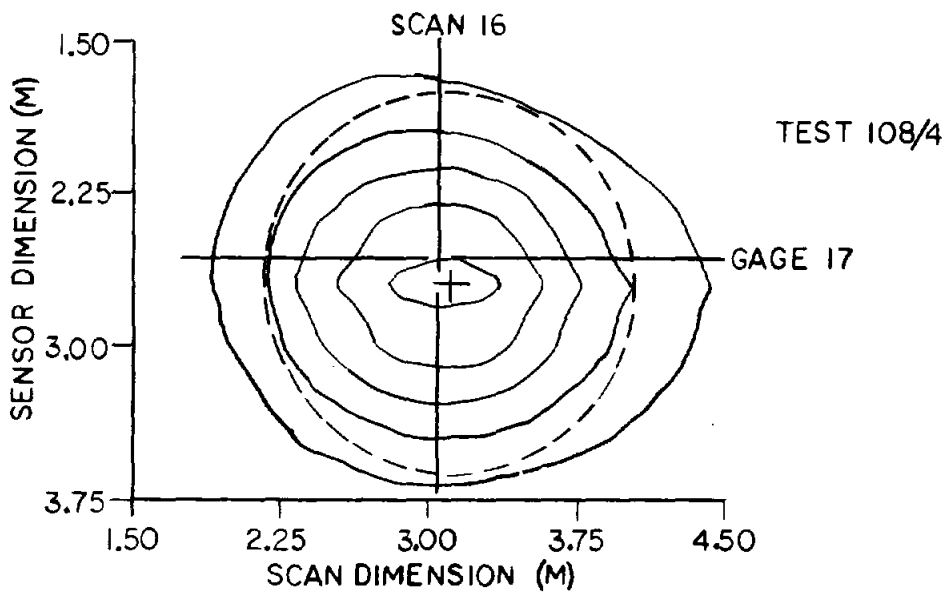
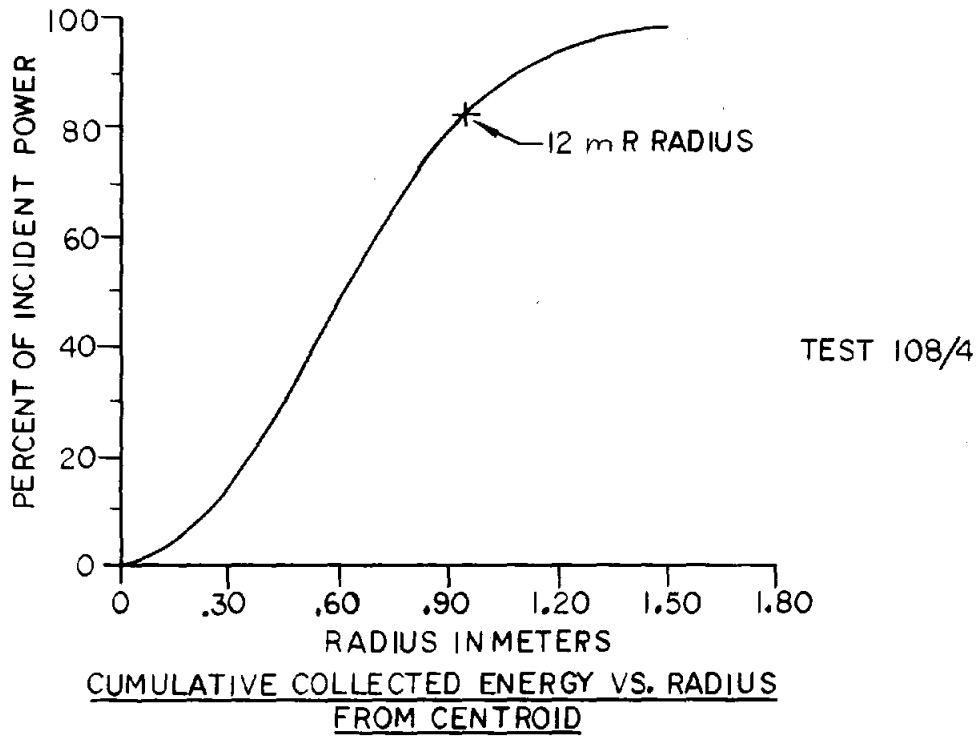


FIGURE 18
CONTOUR PLOT

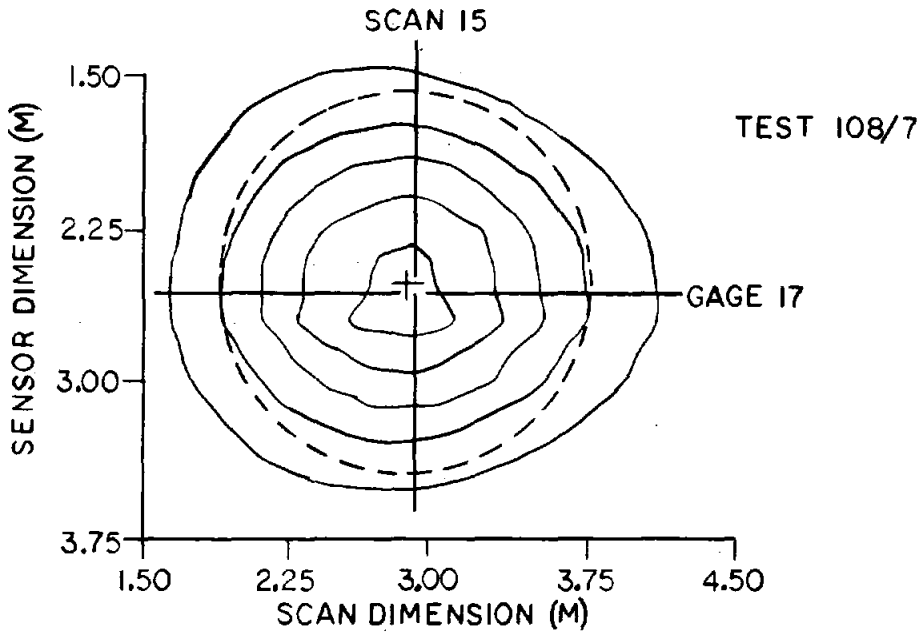
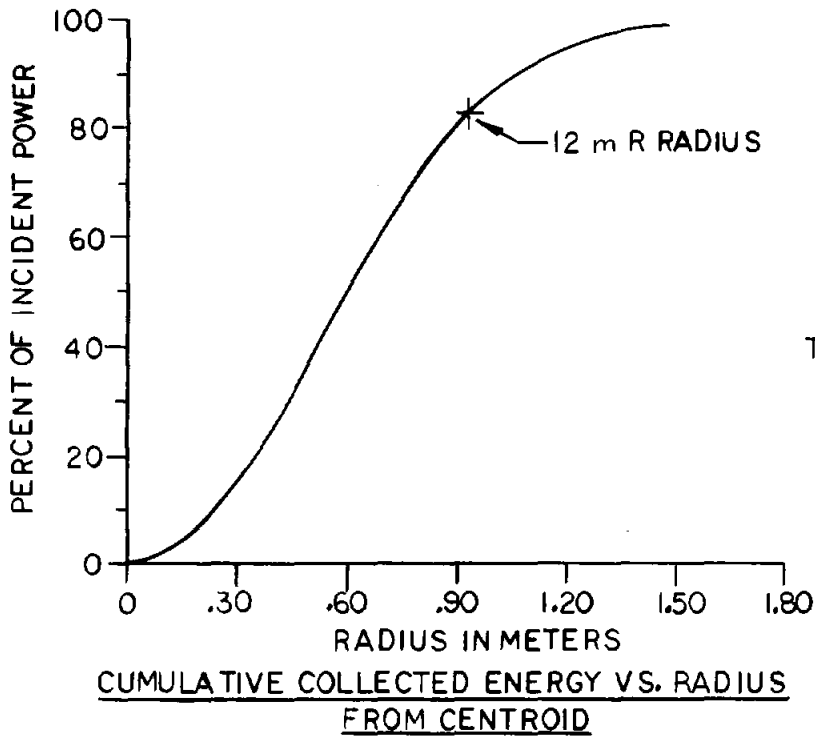


FIGURE 19

CONTOUR PLOT

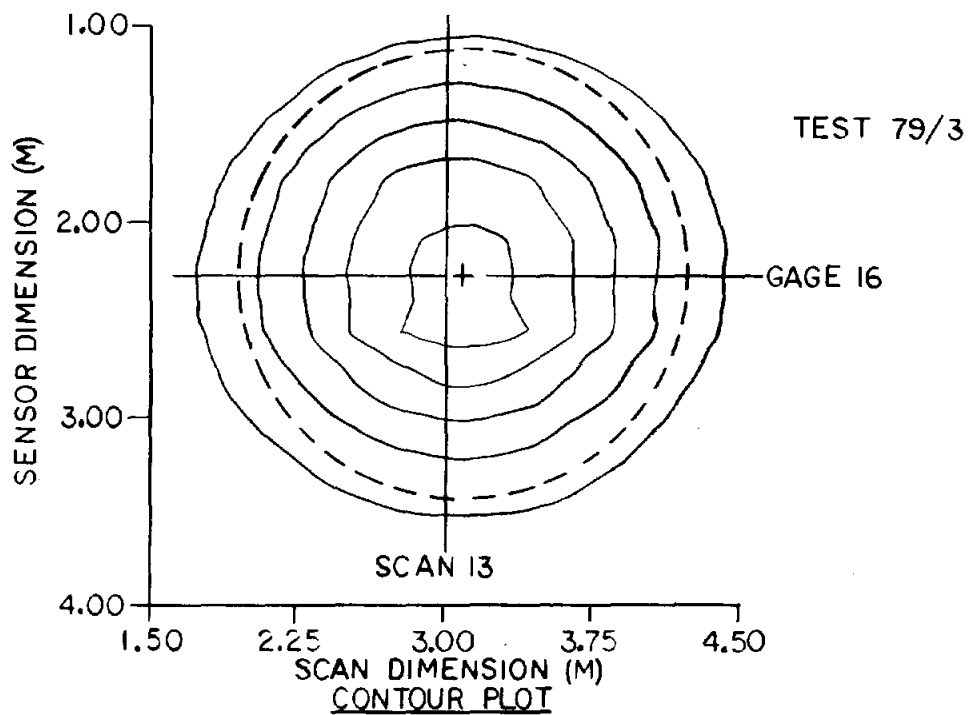
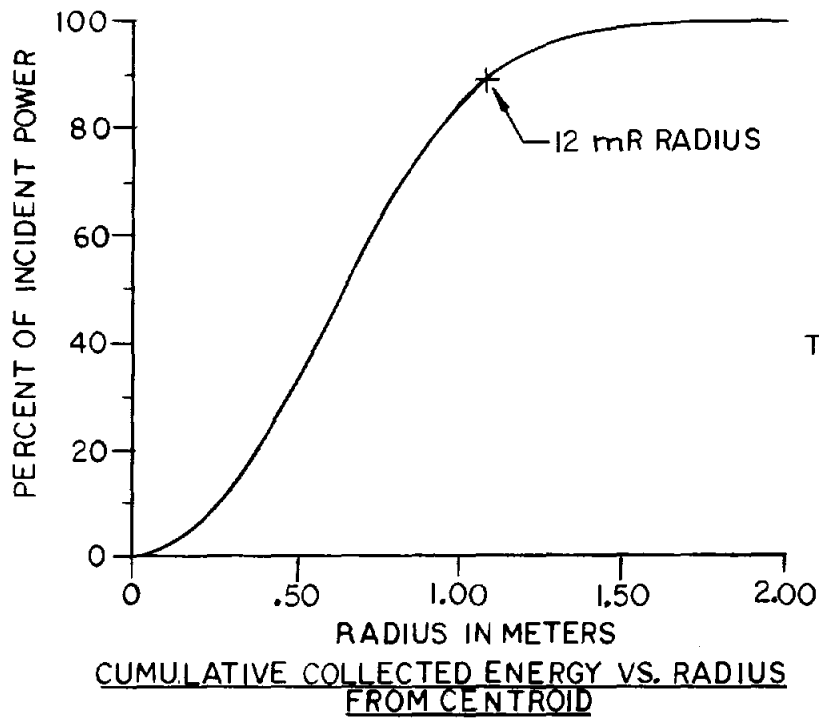
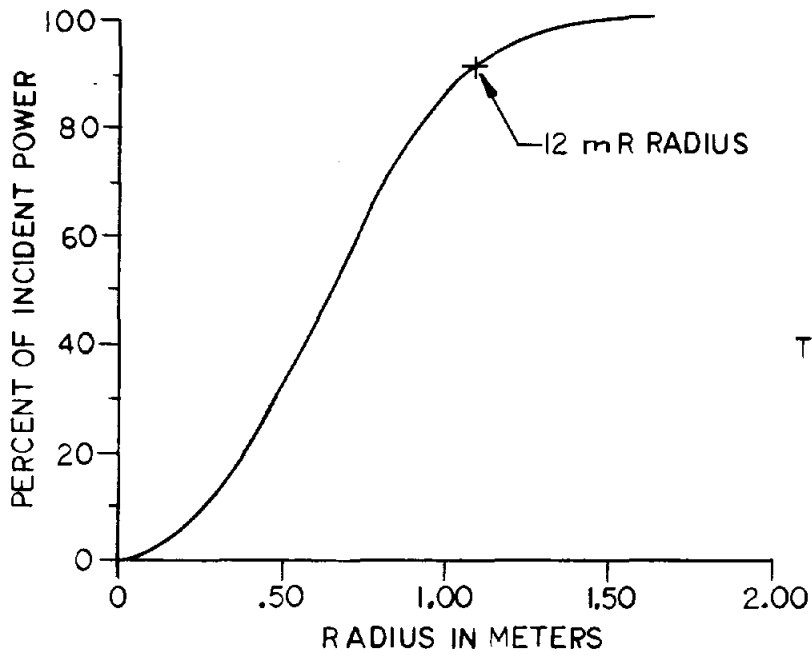
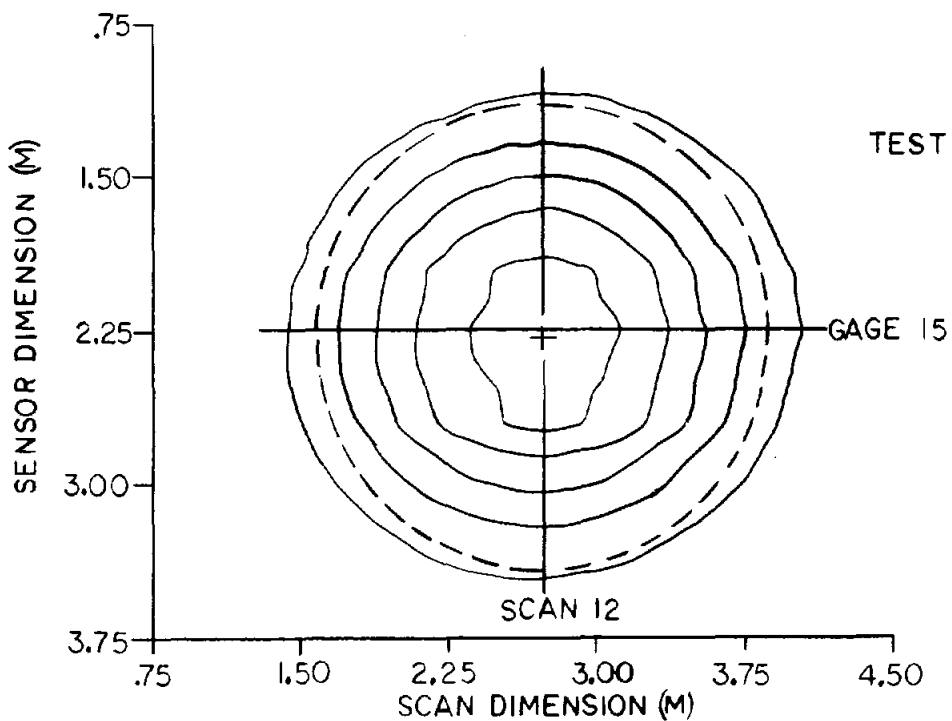


FIGURE 20



TEST 79/5

CUMULATIVE COLLECTED ENERGY VS. RADIUS FROM CENTROID



TEST 79/5

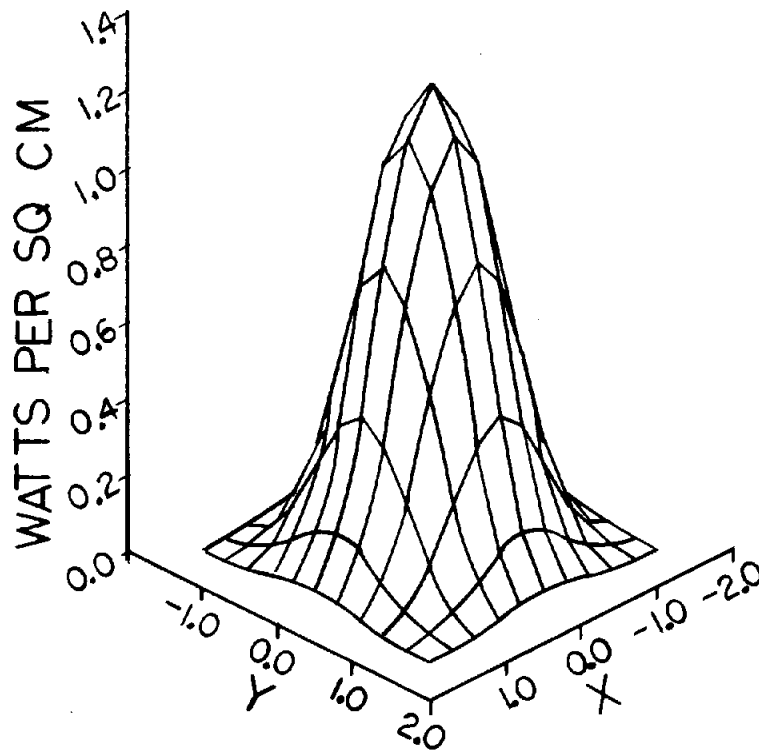
FIGURE 21
CONTOUR PLOT

HELIOS Comparisons

One important task in the heliostat evaluation program development is to verify the computer code HELIOS. HELIOS predictions were made for the test conditions described in the Cal-bar tests, and Figure 22 shows a 3-D contour plot of the prediction for the test run displayed in Figure 21.

A similar HELIOS run was made on all other tests. Since the HELIOS input requires a circular normal error distribution estimate, measured results were matched with calculated results. Using all six test conditions, error input to HELIOS was adjusted to give the best fit on all data. This error distribution half angle was found to be 2 mrad. The matching sequence consisted of first taking a horizontal cross section of the measured data (such as that corresponding to gage 15 in Figure 21) and a vertical cross section of the measured data (such as that corresponding to scan 12 in Figure 21) and comparing the corresponding horizontal and vertical cross sections of the HELIOS calculated results. Comparisons were made by aligning the measured and the corresponding calculated cross section with a least-squares curve-fit matching routine. Figure 23 shows the matching of the horizontal cross section of test 79/5. Figures 24, 25, 26, 27, 28, and 29 give the horizontal and vertical cross section comparisons to an equivalent condition HELIOS calculation using the 2-mrad error distribution input.

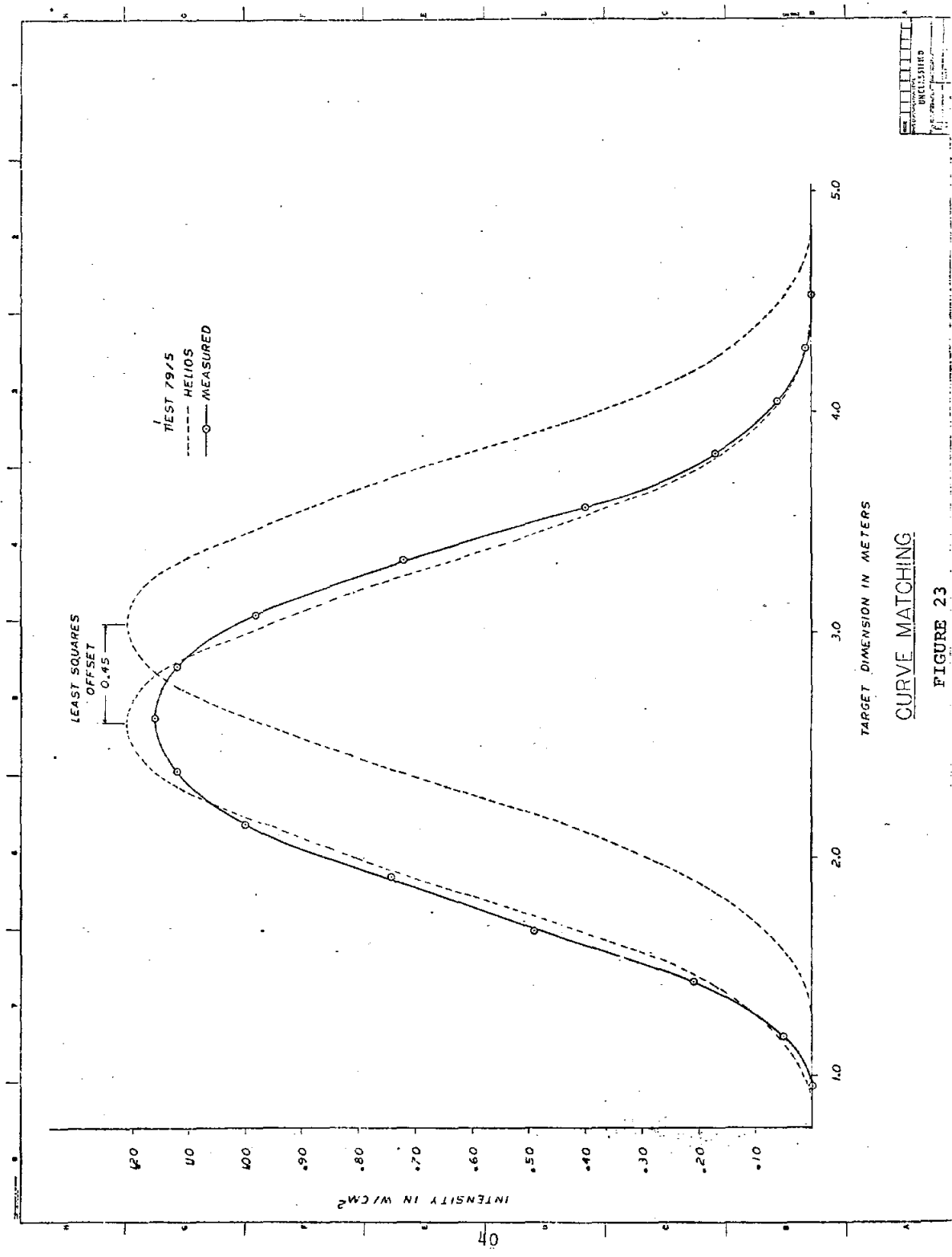
Note that heliostat 108 (see Figures 26 and 27) seemed not to match as well as the other two heliostats tested. The HELIOS prediction matched better with a 2.5-mrad error distribution input. Examination of the data shows a slight ellipticity of the measured beam shape that is not accounted for in the HELIOS circular normal error distribution input. (Improvement in a vertical cross-section comparison may worsen the horizontal cross section comparison and vice versa.) A technique for



ALIGNED FOR DAY 70
DAY= 77.00
TIME=2.0

HELIOS PREDICTION FOR
TEST CONDITIONS
OF HELIOSTAT 79/5

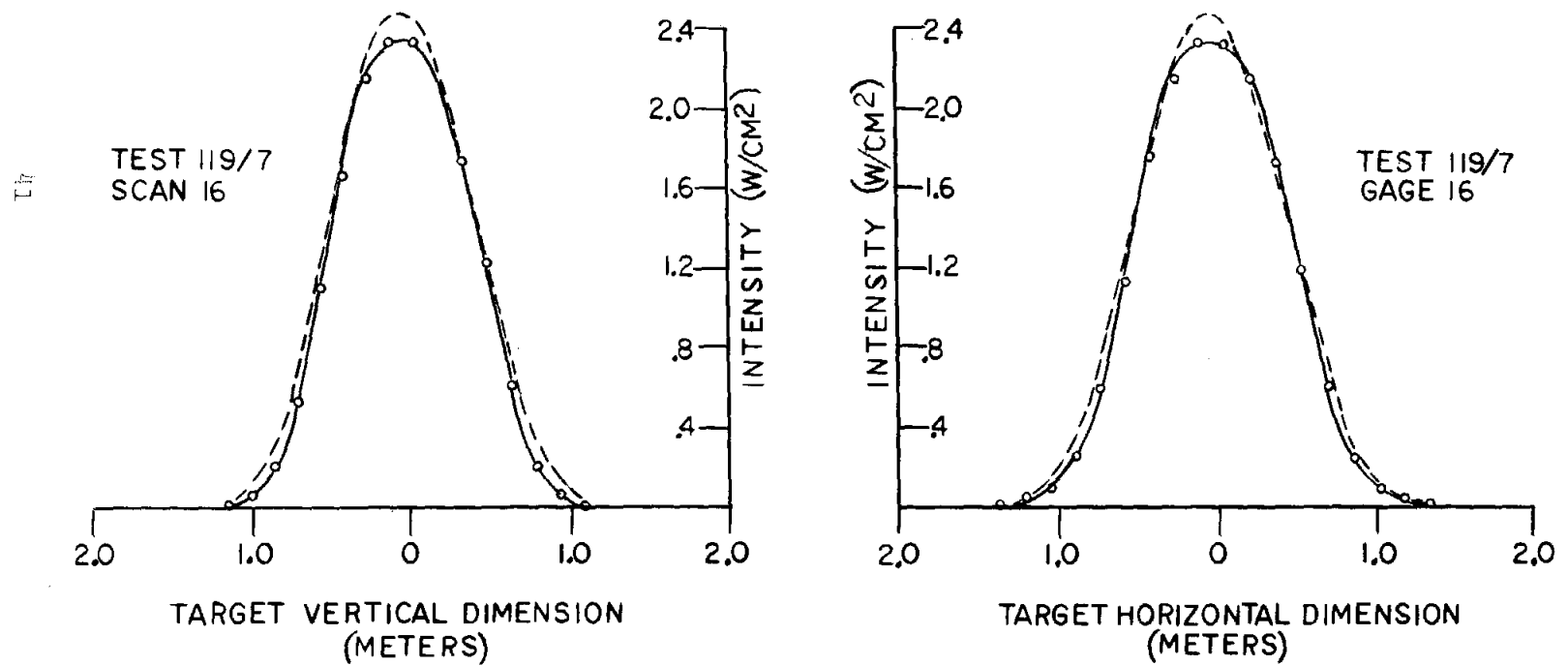
FIGURE 22



CURVE MATCHING

FIGURE 23

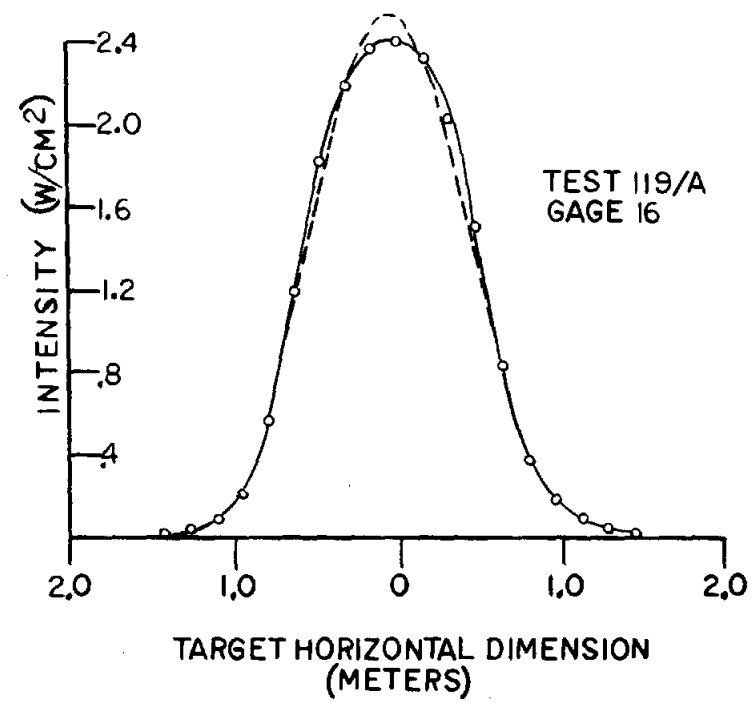
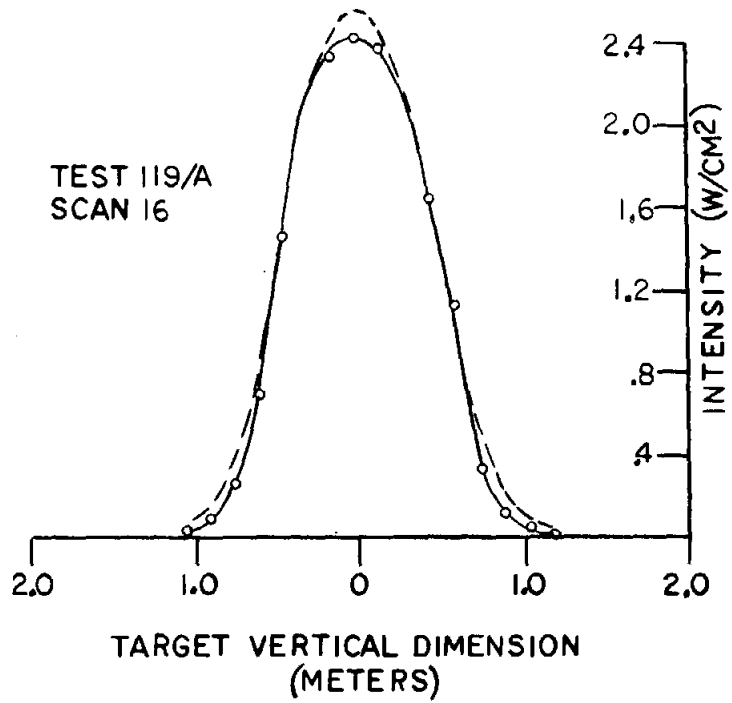
—— MEASUREMENT
- - - - HELIOS PREDICTION 2 mR ERROR



MEASURED VS. PREDICTED BEAM SHAPE
FIGURE 24

42

———— MEASUREMENT
----- HELIOS PREDICTION 2 mR ERROR

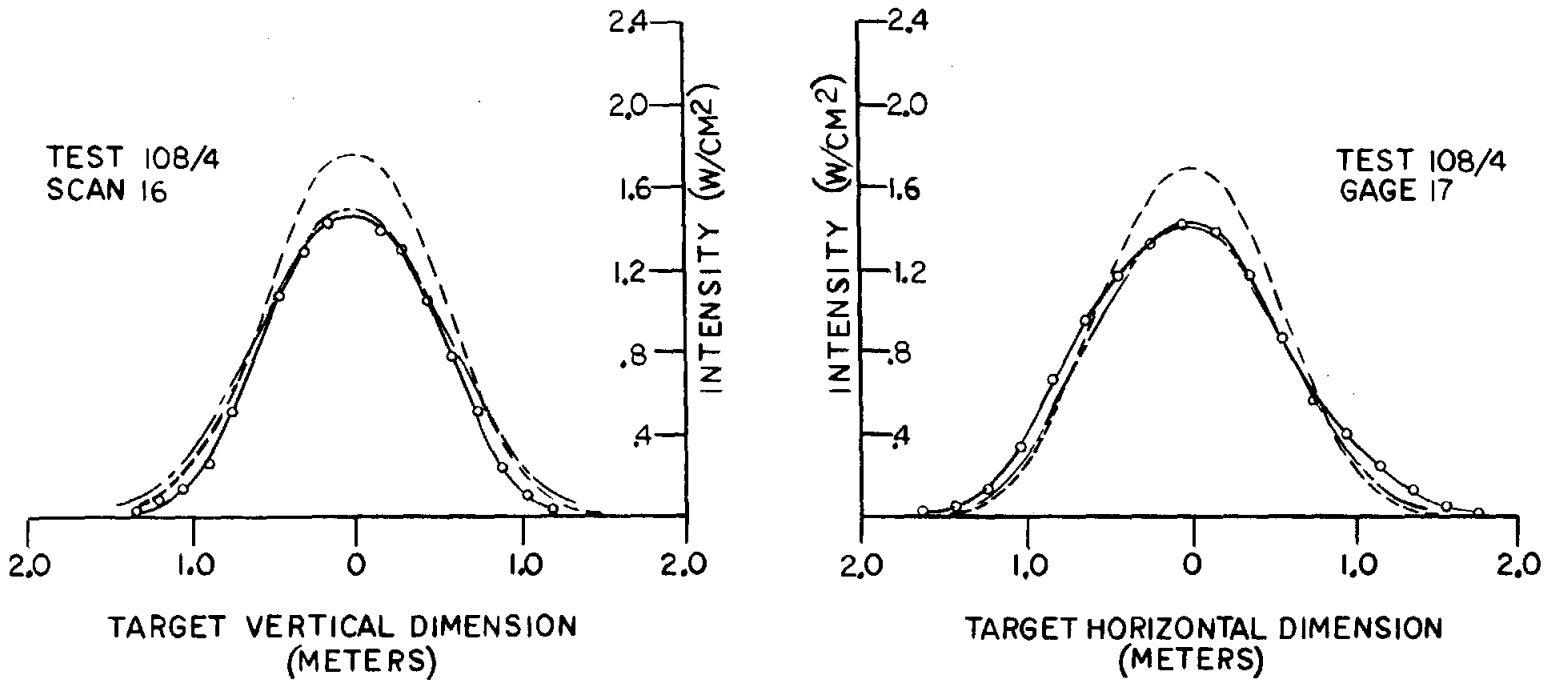


MEASURED VS. PREDICTED BEAM SHAPE

FIGURE 25

37

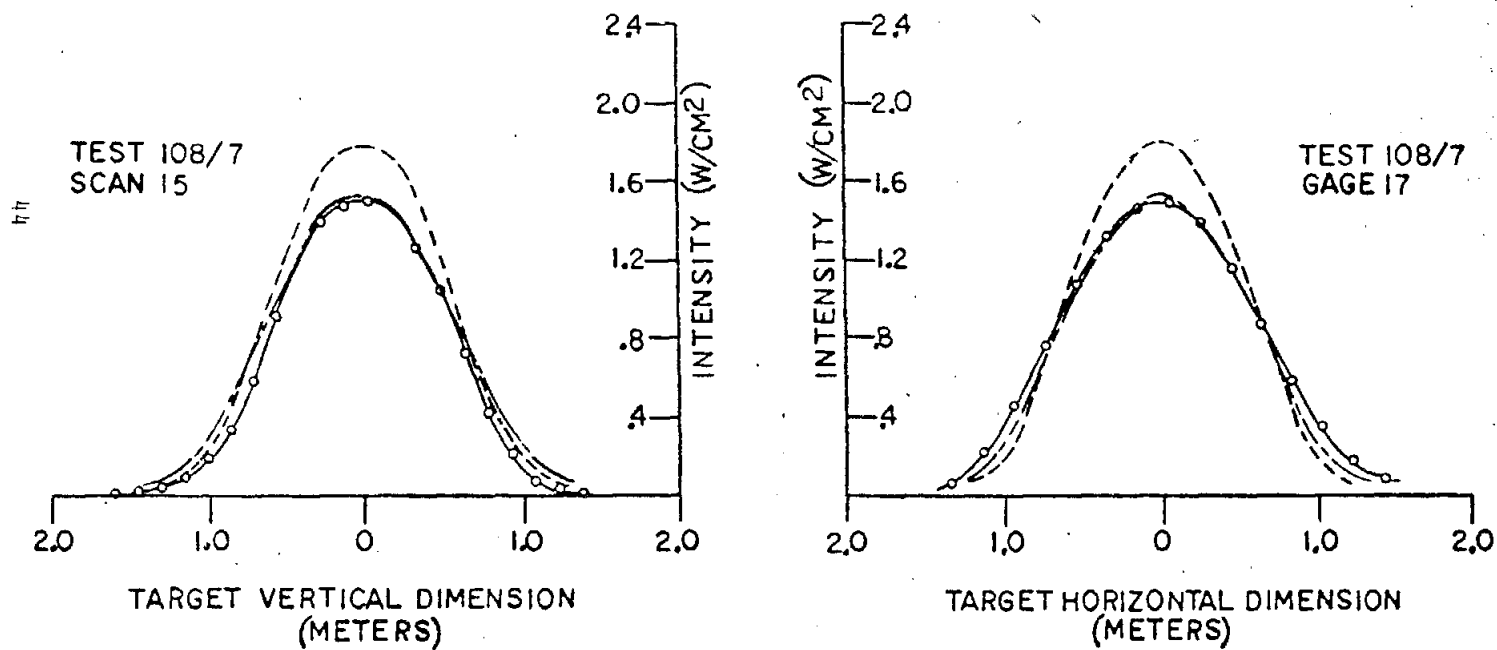
—— MEASUREMENT
- - - HELIOS PREDICTION 2 mR ERROR
- · - HELIOS PREDICTION 2.5 mR ERROR



MEASURED VS. PREDICTED BEAM SHAPE

FIGURE 26

— MEASUREMENT
- - - HELIOS PREDICTION 2 mR ERROR
- · - HELIOS PREDICTION 2.5 mR ERROR

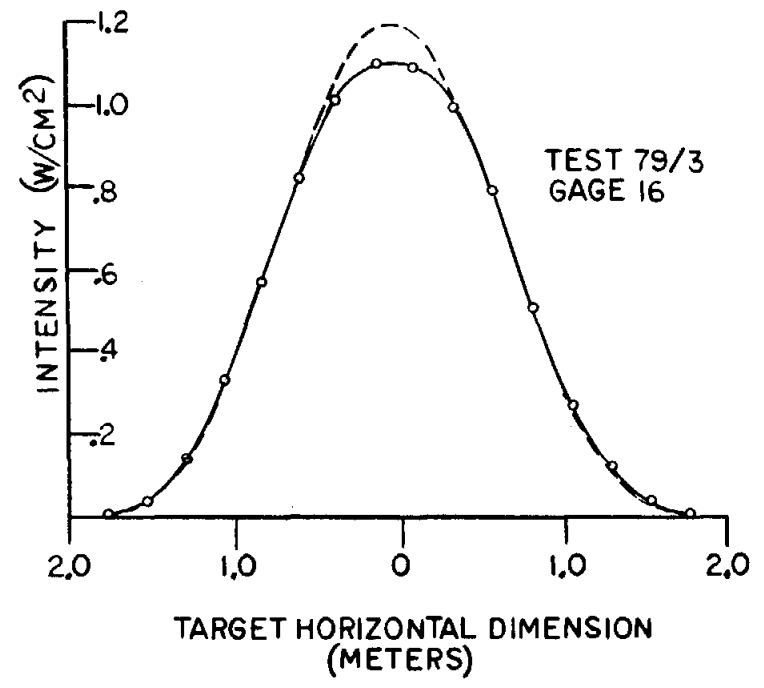
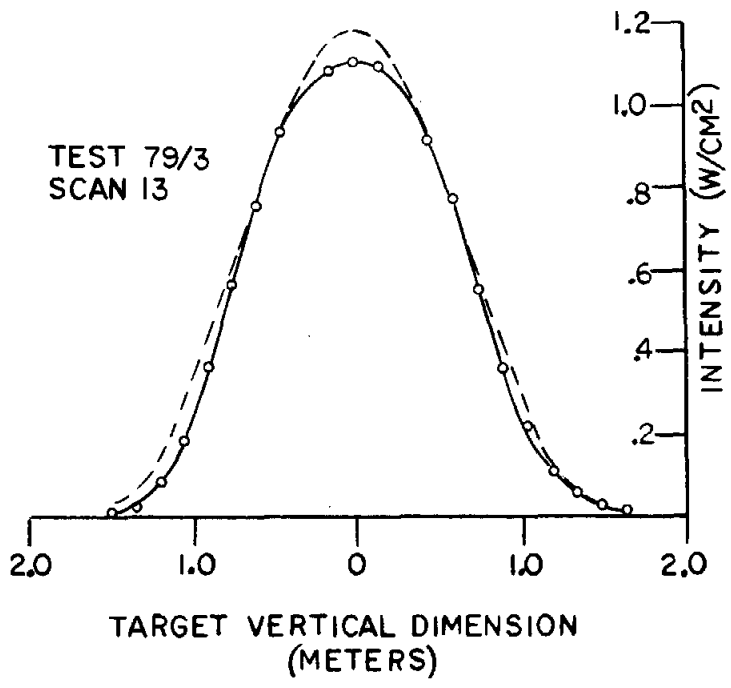


MEASURED VS. PREDICTED BEAM SHAPE

FIGURE 27

45

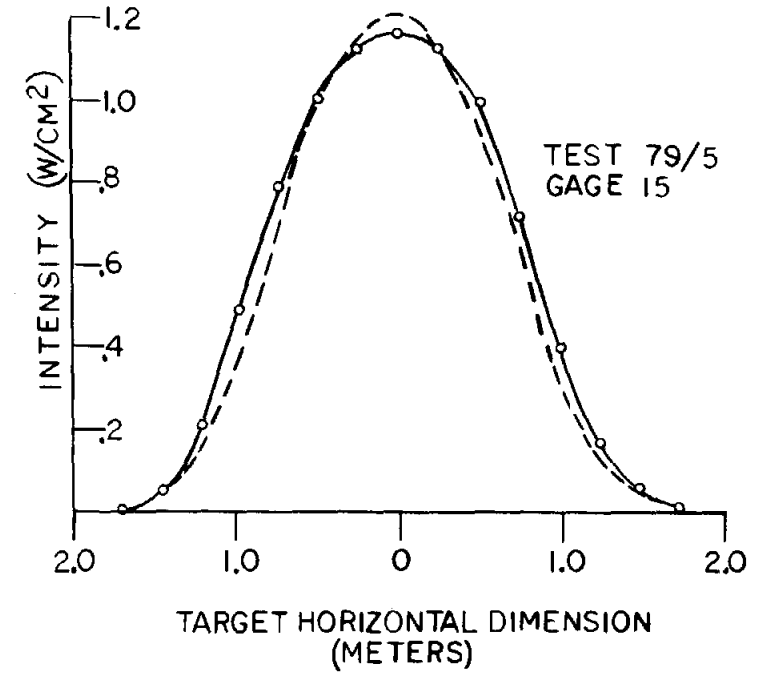
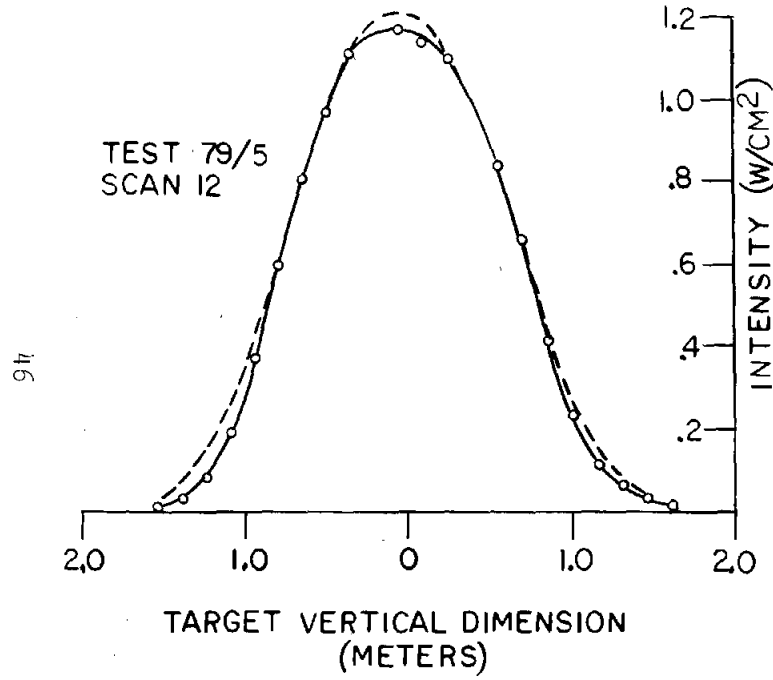
—— MEASUREMENT
- - - - HELIOS PREDICTION 2 m R ERROR



MEASURED VS. PREDICTED BEAM SHAPE

FIGURE 28

———— MEASUREMENT
----- HELIOS PREDICTION 2 mR ERROR



MEASURED VS. PREDICTED BEAM SHAPE

FIGURE 29

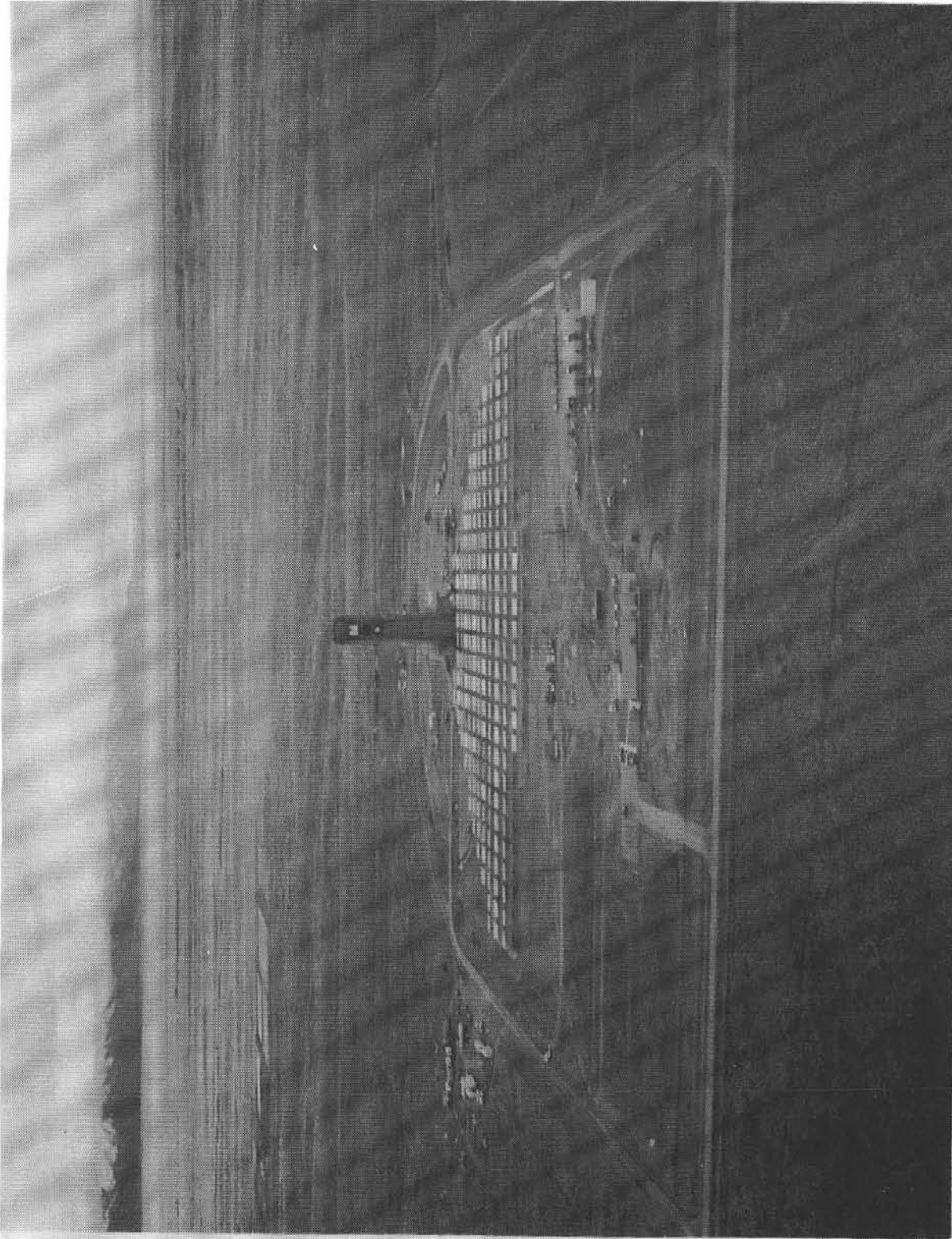
specifying a two-dimensional, elliptic normal error distribution into HELIOS has been completed. The code is being modified to include this capability. Again, the accuracy of these measurements allows only qualitative statements to be made about beam ellipticity and subsequent handling of two-dimensional error distribution inputs into HELIOS.

Summary

The importance of the heliostat subsystem in power plant application has required much attention to heliostat engineering. The intended use of a heliostat array figures as an important input to its design requirements. Quality and performance must be defined with respect to subsystem requirements.

Currently the STTF is one of the most important sources of heliostat performance data. Operational experience is being gained that will develop expertise in this relatively new field. Identification of failure mechanisms has resulted and this information will be used in new designs to improve maintenance and repair requirements.

In addition, the heliostat evaluation program currently underway has promoted development of a versatile Beam Characterization System that will provide information concerning heliostat quality and performance. Use of this improved measurement tool, together with the continually improving computer code HELIOS, will establish a good basis for heliostat evaluation of not only the DOE/Utility sponsored 10-MW_e Pilot Plant prototypes but also other new and advanced heliostat, or concentrator, subsystems.



SOLAR THERMAL TEST FACILITY

References

1. Eason, E. D., "A Heliostat Cost/Performance Model for Trade-off Studies," Division 8122 Memo, Sandia Laboratories, Feb. 22, 1978.
2. Mavis, C. L., "Technical Evaluation of Responses to Request for Quotation D3-3731 for Solar Test Facility Heliostat Array and Control System," Division 8184 Memo, Sandia Laboratories, Dec. 31, 1975.
3. Biggs, F.; C. N. Vittitoe, "On the Evaluation of Heliostats," Division 5231 Memo, Sandia Laboratories, Dec. 5, 1977.
4. Solar Thermal Test Facility Experiment Manual, Division 5713, Sandia Laboratories, October 1977, SAND77-1173.
5. Vittitoe, C. N.; F. Biggs; R. E. Lighthill, HELIOS: A Computer Program for Modeling the Solar Thermal Test Facility-A Users Guide, SAND76-0346, March 1977.
6. Martin-Marietta, "Technical Proposal for Heliostat Array and Control System for 5MW Solar Thermal Test Facility," December 1975.

DISTRIBUTION:

TID-4500-R66, UC62 (316)

Aerospace Corporation
101 Continental Blvd.
El Segundo, CA 90245
Attn: Elliott L, Katz

Acurex Aerotherm
485 Clyde Avenue
Mountain View, CA 94042
Attn: G. J. Neuner

Solar Total Energy Program
American Technological Univ.
P. O. Box 1416
Killeene, TX 76541
Attn: B. L. Hale

Argonne National Laboratory (3)
9700 South Cass Avenue
Argonne, Ill 60439
Attn: R. G. Matlock
W. W. Schertz
Roland Winston

Atlantic Richfield Co.
515 South Flower Street
Los Angeles, CA 90071
Attn: H. R. Blieden

Barber Nichols Engineering
6325 W. 55th Avenue
Arvada, CO 80002
Attn: R. G. Olander

Battelle Memorial Institute
Pacific Northwest Laboratory
P. O. Box 999
Richland, WA 99352
Attn: K. Drumheller

Brookhaven National Laboratory
Associated Universities, Inc.
Upton, LI, NY 11973
Attn: J. Blewett

Congressional Research Service
Library of Congress
Washington, DC 20540
Attn: H. Bullis

Del Manufacturing Co.
905 Monterey Pass Road
Monterey Park, CA 91754
Attn: M. M. Delgado

Desert Research Institute
Energy Systems Laboratory
1500 Buchanan Blvd
Boulder City, NV 89005
Attn: Jerry O. Bradley

DSET
Black Canyon Stage
P. O. Box 185
Phoenix, AZ 85029
Attn: Gene A Zerlaut

Honorable Pete V. Domenici
Room 405
Russel Senate Office Bldg.
Washington, DC 20510

Edison Electric Institute
90 Park Avenue
New York, NY 10016
Attn: L. O. Elsaesser,
Director of Research

Energy Institute
1700 Las Lomas
Albuquerque, NM 87131
Attn: T. T. Shishman

EPRI
3412 Hillview Avenue
Palo Alto, CA 94303
Attn: J. E. Bigger

General Atomic
P. O. Box 81608
San Diego, CA 92138
Attn: Alan Schwartz

General Electric Company
Valley Forge Space Center
Valley Forge, PA 19087
Attn: Walt Pijawka

General Electric Co.
P. O. Box 8661
Philadelphia, PA 19101
Attn: A. J. Poche

DISTRIBUTION (cont.)

Georgia Institute of Technology
School of Mechanical Engineering
Atlanta, GA 30332
Attn: S. Peter Kezios,
President
American Society of
Mechanical Engineers

Georgia Institute of Technology
Atlanta, GA 30332
Attn: J. D. Walton

Georgia Power Company
Atlanta, GA 30302
Attn: Mr. Walter Hensley
Vice President
Economic Services

Grumman Corporation
4175 Veterans Memorial Highway
Ronkonkoma, NY 11779
Attn: Ed Diamond

Hexcel
11711 Dublin Blvd.
Dublin, CA 94566
Attn: George P. Branch

Industrial Energy Control Corp.
118 Broadway
Hillsdale, NJ 07675
Attn: Peter Groome

Jet Propulsion Laboratory
4800 Oak Grove Drive
Pasadena, CA 91103
Attn: V. C. Truscello

Kingston Industries Corp.
205 Lexington Avenue
New York, NY 10016
Attn: Ken Brandt

Lawrence Berkley Laboratory
University of California
Berkley, CA 94720
Attn: Mike Wallig

Lawrence Livermore Laboratory
University of California
P. O. Box 808
Livermore, CA 94500
Attn: W. C. Dickinson

Los Alamos Scientific Laboratory
Los Alamos, NM 87545
Attn: J. D. Balcomb
C. D. Bankston
D. P. Grimmer

Honorable Manuel Lujan
1324 Longworth Building
Washington, DC 20515

Mann-Russell Electronics, Inc.
1401 Thorne Road
Tacoma, WA 98421
Attn: G. F. Russell

Martin Marietta Aerospace
P. O. Box 179
Denver, CO 80201
Attn: R. C. Rozycki
P. R. Brown

McDonnell-Douglas Astronautics Co
5301 Bolsa Avenue
Huntington Beach, CA 92647
Attn: Don Steinmeyer
R. McFee
J. Blackmon

NASA-Lewis Research Center
Cleveland, OH 44135
Attn: R. Hyland

New Mexico State University
Solar Energy Department
Las Curces, NM 88001

Oak Ridge Associated Universities
P. O. Box 117
Oak Ridge, TN 37830
Attn: A. Roy

DISTRIBUTION (cont.)

Oak Ridge National Laboratory
P. O. Box Y
Oak Ridge, TN 37830
Attn: J. R. Blevins
C. V. Chester
J. Johnson
S. I. Kaplan

Office of Technology Assessment
U. S. Congress
Washington, DC 20510
Attn: Dr. Henry Kelly

Omnium G
1815 Orangethorpe Park
Anaheim, CA 92801
Attn: Ron Derby
S. P. Lazzara

PRC Energy Analysis Company
7600 Old Springhouse Road
McLean, VA 22102
Attn: K. T. Cherian

Rocket Research Company
York Center
Redmond, WA 98052
Attn: R. J. Stryer

Honorable Harold Runnels
1535 Longworth Building
Washington, DC 20515

Honorable Harrison H. Schmitt
Room 1251
Dirksen Senate Office Bldg.
Washington, DC 20510

Scientific Atlanta, Inc.
3845 Pleasantdale Road
Atlanta, GA 30340
Attn: Andrew L. Blackshaw

Sensor Technology, Inc.
21012 Lassen Street
Chatsworth, CA 91311
Attn: Irwin Rubin

Solar Energy Technology
Rocketdyne Division
6633 Canoga Avenue
Canoga Park, CA 91304
Attn: J. M. Friefeld

Solar Energy Research Institute
1536 Coal Blvd.
Golden, CO 80401
Attn: C. J. Bishop
Ken Brown
B. L. Butler
Frank Krieth
Charles Grosskruetz
B. P. Gupta (5)
A. Rabl

Solar Kinetics Inc.
P. O. Box 10764
Dallas, TX 75207
Attn: Gus Hutchinson

STTF Users Association (10)
Suite 1507
First National Bank Bldg. East
Albuquerque, NM 87108
Attn: F. G. Smith

Southwest Research Institute
P. O. Box 28510
San Antonio, TX 78284
Attn: Danny M. Deffenbaugh

Stanford Research Institute
Menlo Park, CA 94025
Attn: Arthur J. Slemmons

Stanford University
Mechanical Engineering Dept.
Palo Alto, CA 94305
Attn: D. E. Arvizu

Stone & Webster
Box 5406
Denver, CO 80217
Attn: V. O. Staub

Sun Gas Company
Suite 800, 2 No. Pk. E
Dallas, TX 75231
Attn: R. C. Clark

Sundstrand Electric Power
4747 Harrison Avenue
Rockford, IL 61101
Attn: A. W. Adam

DISTRIBUTION (cont.)

Sunsearch, Inc.
669 Boston Post Road
Gilford, CT 06437
Attn: E. M. Barber, Jr.

Suntec Systems Inc.
21405 Hamburg Avenue
Lakeville, MN 55044
Attn: J. H. Davidson

Swedlow, Inc.
12122 Western Avenue
Garden Grove, CA 92645
Attn: E. Nixon

TEAM Inc.
8136 Ola Keene Mill Road
Springfield, VA 22152

U. S. Department of Energy
Agricultural & Industrial
Process Heat Conservation &
Solar Application
Washington, DC 20545
Attn: W. W. Auer
J. Dollard

U. S. Department of Energy (3)
Albuquerque Operations Office
P. O. Box 5400
Albuquerque, NM 87185
Attn: K. K. Nowlin
G. Pappas
J. R. Roder

U. S. Department of Energy
Division of Energy Storage
Systems
Washington, DC 20545
Attn: C. J. Swet

U. S. Department of Energy
Los Angeles Operations Office
350 S. Figueroa Street,
Suite 285
Los Angeles, CA 90071
Attn: Fred A. Glaski

U. S. Department of Energy (9)
Division of Central Solar
Technology
Washington, DC 20545
Attn: R. H. Annan
G. W. Braun
J. Coleman
M. U. Gutstein
G. M. Kaplan
Lou Melamed
J. E. Rannels
M. E. Resner
J. Weisiger

U. S. Department of Energy
San Francisco Operations Office
1333 Broadway, Wells Fargo Bldg.
Oakland, CA 94612
Attn: Jack Blasy

University of Delaware
Institute of Energy Conversion
Newark, DE 19711
Attn: K. W. Boer

University of New Mexico (2)
Department of Mechanical Eng.
Albuquerque, NM 87113
Attn: W. A. Cross
M. W. Wilden

Watt Engineering Ltd.
RR1, Box 183 1/2
Cedaredge, CO 81413
Attn: A. D. Watt

Western Control Systems
13640 Silver Lake Drive
Poway, CA 92064
Attn: L. P. Capiello

Westinghouse Electric Corp.
P. O. Box 10864
Pittsburgh, PA 15236
Attn: J. Buggy

DISTRIBUTION (cont.)

1100	C. C. Broyles	3141	T. L. Werner
1472	L. G. Rainhart	3151	W. L. Garner (3)
1500	W. A. Gardner		For DOE/TIC
1520	T. L. Pace		(Unlimited Release)
1530	W. E. Caldes		
1540	R. L. Brin		
1550	F. W. Neilson		
1552	O. N. Burchett		
2300	J. C. King		
2320	K. L. Gillespie		
2323	C. M. Gabriel		
2324	L. W. Schulz		
2326	G. M. Heck		
3161	J. E. Mitchell		
3600	R. W. Hunnicutt		
	Attn: 3640 H. H. Pastorius		
3700	J. C. Strassell		
4000	A. Narath		
4531	J. H. Renken		
4700	J. H. Scott		
4710	G. E. Brandvold		
4713	B. W. Marshall (50)		
4714	R. P. Stromberg (5)		
4715	R. H. Braasch		
4719	D. G. Schueler		
4720	V. L. Dugan		
4721	J. V. Otts		
4722	J. F. Banas		
4723	W. P. Schimmel		
4725	J. A. Leonard		
4730	H. M. Stoller		
5512	H. C. Hardee		
5520	T. B. Lane		
5524	R. T. Othmer		
5600	D. B. Schuster		
5630	R. C. Maydew		
5834	D. M. Mattox		
	Attn: 5831 N. M. Magnani		
5840	H. J. Saxton		
	Attn: 5810 R. G. Kepler		
	5820 R. L. Schwoebel		
	5830 M. J. Davis		
5844	F. P. Gerstle		
	Attn: 5842 J. N. Sweet		
	5846 E. K. Beauchamp		
8100	L. Gutierrez		
8266	E. A. Aas		
8450	R. C. Wayne (10)		
8451	W. G. Wilson (5)		
8452	A. C. Skinrood (5)		
8453	J. D. Gilson		
8470	C. S. Selvage		